Mars Science Laboratory Curiosity Rover Megaripple Crossings up to Sol 710 in Gale Crater

Raymond E. Arvidson
McDonnell Center for the Space Sciences, Department of Earth and Planetary Sciences, Washington University in St. Louis, St. Louis, Missouri 63130
e-mail: arvidson@wunder.wustl.edu
Karl D. Iagnemma
Robotic Mobility Group, Massachusetts Institute of Technology, Cambridge, Massachusetts 02139
e-mail: kdi@mit.edu
Mark Maimone
California Institute of Technology/ Jet Propulsion Laboratory, Pasadena, California 91011
e-mail: mark.maimone@jpl.nasa.gov
Abigail A. Fraeman
Division of Geological and Planetary Sciences, California Institute of Technology, Pasadena, California 91125
e-mail: afraeman@caltech.edu
Feng Zhou
McDonnell Center for the Space Sciences, Department of Earth and Planetary Sciences, Washington University in St. Louis, St. Louis, Missouri 63130
e-mail: chow@wunder.wustl.edu
Matthew C. Heverly and Paolo Bellutta
California Institute of Technology/ Jet Propulsion Laboratory, Pasadena, California 91011
e-mail: matthew.c.heverly@jpl.nasa.gov, bellutta@helios.jpl.nasa.gov
David Rubin
Department of Earth and Planetary Sciences, University of California at Santa Cruz, Santa Cruz, California 91125
e-mail: drubin@ucsc.edu
Nathan T. Stein
McDonnell Center for the Space Sciences, Department of Earth and Planetary Sciences, Washington University in St. Louis, St. Louis, Missouri 63130
e-mail: n.stein@wustl.edu
John P. Grotzinger
Division of Geological and Planetary Sciences, California Institute of Technology, Pasadena, California 91125
e-mail: grotz@gps.caltech.edu
Ashwin R. Vasavada
California Institute of Technology/ Jet Propulsion Laboratory, Pasadena, California 91011
e-mail: ashwin.r.vasavada@jpl.nasa.gov

Received 5 June 2015; accepted 23 December 2015

After landing in Gale Crater on August 6, 2012, the Mars Science Laboratory Curiosity rover traveled across regolith-covered, rock-strewn plains that transitioned into terrains that have been variably eroded, with valleys partially filled with windblown sands, and intervening plateaus capped by well-cemented sandstones that have been fractured and shaped by wind into outcrops with numerous sharp rock surfaces. Wheel punctures and tears caused by sharp rocks while traversing the plateaus led to directing the rover to traverse in valleys where sands would cushion wheel loads. This required driving across a megaripple (windblown, sand-sized deposit covered by coarser grains) that straddles a narrow gap and several extensive megaripple deposits that accumulated in low portions of valleys. Traverses across megaripple deposits led to mobility difficulties, with

Direct correspondence to: Raymond Arvidson, e-mail: arvidson@wunder.wustl.edu

View this article online at wileyonlinelibrary.com • DOI: 10.1002/rob.21647

sinkage values up to approximately 30% of the 0.50 m wheel diameter, resultant high compaction resistances, and rover-based slip up to 77%. Analysis of imaging and engineering data collected during traverses across megaripples for the first 710 sols (Mars days) of the mission, laboratory-based single-wheel soil experiments, full-scale rover tests at the Dumont Dunes, Mojave Desert, California, and numerical simulations show that a combination of material properties and megaripple geometries explain the high wheel sinkage and slip events. Extensive megaripple deposits have subsequently been avoided and instead traverses have been implemented across terrains covered with regolith or thin windblown sand covers and megaripples separated by bedrock exposures.

1. INTRODUCTION

The NASA Mars Science Laboratory Curiosity rover has been traversing across the northern plains of Gale Crater and the base of Mount Sharp since the vehicle landed on August 6, 2012 (Grotzinger et al., 2012; Vasavada et al., 2015) (Figures 1, 2). Data acquired by Curiosity's remote sensing and in situ instruments show that strata underlying the traversed terrains consist of sedimentary rocks deposited in an ancient fluvial-deltaic-lacustrine system (Grotzinger et al., 2014; Williams et al., 2013). During the first approximately 480 sols (Mars days), the rover mainly traversed across terrain called hummocky plains, with a relatively thin, dominantly sand- to clay-sized regolith cover over bedrock, with rocks of a variety of sizes dispersed across the landscape (Arvidson et al., 2014). For reference, regolith on Mars is defined as loose or loosely consolidated particulate material generated by impact, physical and chemical weathering of local bedrock, and the addition of windblown granule, sand, silt, and clay-sized particles (Arvidson, Gooding, & Moore, 1989; Moore, 1987).

As Curiosity continued traversing to the southwest on the way to Mount Sharp the terrain transitioned to plateaus, and intervening valleys formed as wind erosion carved into the plains. To help define safe traverses, detailed terrain mapping was performed using images from the HiRISE instrument on the Mars Reconnaissance Orbiter (McEwen et al., 2007), along with digital elevation maps generated from stereo HiRISE data. Mapped units included (a) hummocky plains, (b) dissected or rugged terrain dominated by plateaus and intervening valleys, and (c) relatively bright, striated bedrock units typically found on valley floors. Valley floors were mapped as covered by regolith, with windblown megaripples located in the lowest portions of valleys, and in narrow gaps between plateaus.

Remote sensing and contact science measurements acquired by Curiosity show that megaripples consist of loosely consolidated, poorly sorted, angular sand-sized particles of basaltic composition, with a thin armor of coarse granule-sized to sand-sized particles, variably covered by a thin airfall dust deposit (Blake et al., 2013; Fraeman et al., 2015; Sullivan & Zimbelman, 2015). Megaripples are the most common windblown bedform on Mars and formed as the poorly sorted sediment supply was differentially sorted by winds, leaving coarser grains stranded on ripple surfaces (Sullivan & Zimbelman, 2015). They likely formed during rare high-velocity wind events.

Curiosity observations show that the rugged terrain plateaus are capped by well-cemented sandstone bedrock shaped by wind into sharp surfaces. When unavoidably driven over by Curiosity, the sharp rocks punctured the thin (0.75-mm-thick skin) aluminum wheels at an unacceptably high rate. Traverses were then preferentially planned and implemented in valleys, with the hypothesis that the regolith cover and sand-dominated megaripples on valley floors would cushion the wheels and reduce wheel wear and tear rates. This approach occasionally led to traverses across megaripple deposits that produced high wheel sinkages (~0.15 m, or ~30% of the 0.5 m wheel diameter), increased compaction resistances, and rover-based slip values (up to 77%) that exceeded onboard safety thresholds.

This paper focuses on a summary of traverses across a single megaripple straddling Dingo Gap, together with traverses across several areally extensive megaripple deposits (Figure 2). The paper covers drives through the first 710 sols of the Curiosity mission, with an emphasis on understanding the interactions between the vehicle and the traversed megaripple field geometries and material properties, together with implications for future traverses within Gale Crater. The sol range is appropriate because after sol 710 it was decided to drive around extensive megaripple fields to avoid possible embedding events.

2. CURIOSITY ROVER AND OPERATIONS OVERVIEW

Curiosity has a mass of 899 kg and employs six-wheel drive, with the outer four wheels capable of turning about vertical axes using azimuthal actuators (Figures 1 and 3). The rover has a rocker-bogie suspension system designed to go over obstacles while maintaining low rover tilts and evenly distributing the loads among the wheels (Bickler, 1988). Wheels are 0.50 m in diameter, 0.40 m wide, and have 0.00075-m-thick aluminum skins in between 0.007-m-high grousers (Haggert & Waydo, 2008). One section of each wheel has the letters JPL in Morse code cut into the wheel surface, thereby providing a unique wheel track imprint in deformable materials, such as regolith and windblown sands. Actuators were chosen for turning and driving purposes that provide torque values that were estimated to be several times higher than typically needed.

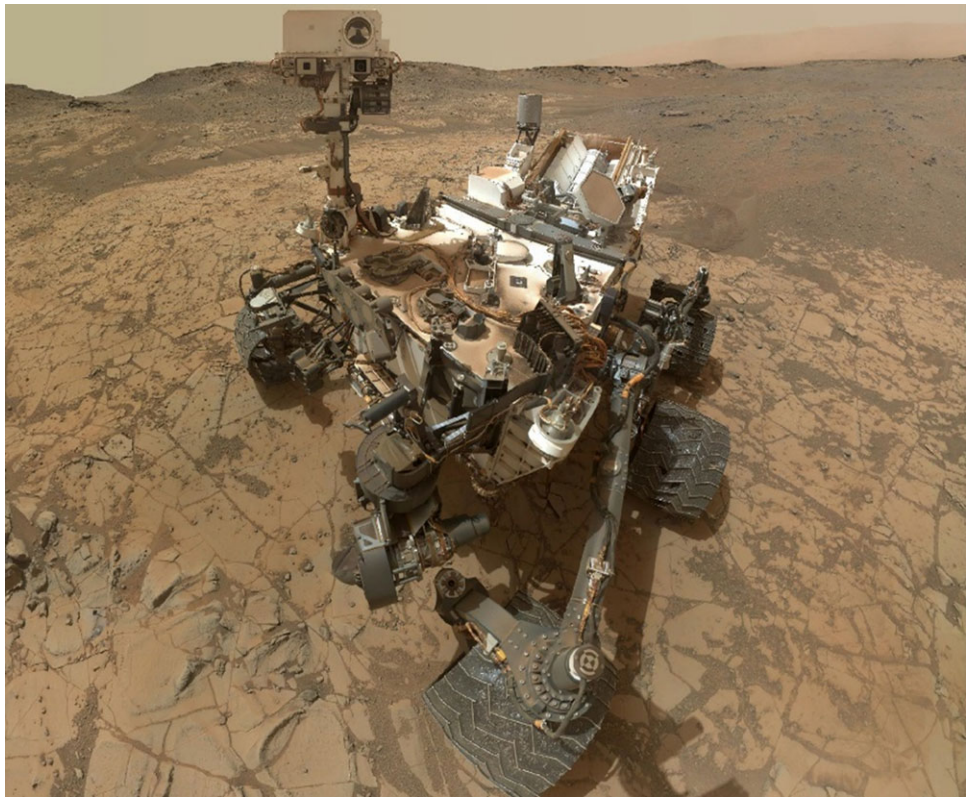

Figure 1. Curiosity self-portrait mosaic acquired by the Mars Hand Lens Imager (Edgett et al., 2012) on the robotic arm on sols 868 to 884. The rover was located in Pahrump Hills, to the south of the megaripple crossing locations presented in this paper. Bedrock underlying the rover has been interpreted to have been deposited in an ancient lake environment. The plateau in the upper left portion of the image is capped by sandstone bedrock interpreted to have formed in a fluvial environment. See Grotzinger et al. (2012) for a description of the other science instruments on Curiosity. Curiosity product IDs in this and other figure captions are listed in Table I. The products are available from the NASA Planetary Data System.

Drives are accomplished along Ackerman arcs of given radii of curvature using the azimuthal actuators to set the curvature, along with appropriate drive actuator currents to achieve wheel angular velocities needed to maintain the commanded drive path. Autonavigation using body-mounted hazard avoidance stereo cameras (front and rear Hazcams; Maki et al., 2012) can be used to automatically detect and move around obstacles (Maimone, Cheng, & Matthies, 2007). Visual odometry, in which periodic stereo imaging of the surrounding terrain taken by the mast-mounted Navcams (Maki et al., 2012), can be used to determine actual drive distances and directions, which the rover can then use to correct path vectors relative to commanded values (Maimone et al., 2007). Visual odometry also allows calculation of rover-based slip and skid values. Slip in percentage is defined as:

$$Slip = 100 * (1 - actual\ distance\ traveled / commanded\ distance) \quad (1)$$

Slip becomes skid when the actual distance traveled is greater than the commanded distance, with a resultant negative value. To avoid embedding events, slip values are computed onboard and automatically compared to preset threshold values, as shown in Table II. Traverses are automatically stopped if a single, or "fast" slip, value exceeds a set threshold. The rover also stops its traverse if "slow" slip values exceed a threshold slip setting over a consecutive number (called persistence) of slip measurements. Threshold slip values (~70 to 80%) have been set based on experience from driving in sands at the Jet Propulsion Laboratory's Mars Yard and the Dumont Dunes, Mojave Desert (Heverly et al., 2013), tempered by the permanent embedding (~100% slip) of the Mars Exploration Rover, Spirit, in loose sands in Gusev Crater (Arvidson et al., 2010). Maximum slip values for each of the traverses discussed in this paper are shown in Table II. Drives were automatically halted by Curiosity on sols 672, 709, and 710 because "fast" slip values exceeded threshold limits set for the traverses.

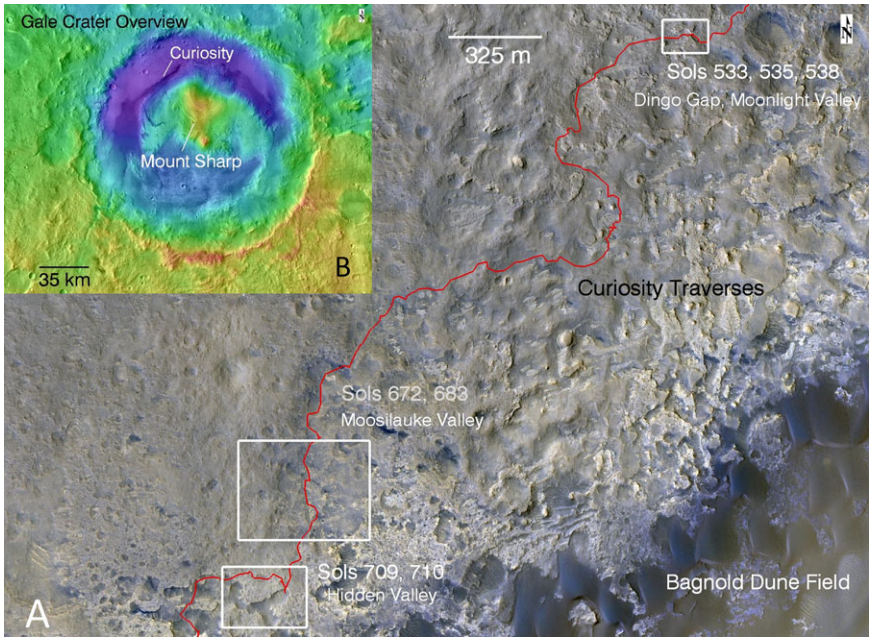

Figure 2. A. HiRISE image mosaic showing Curiosity's traverses (red line) from crossing the single megaripple straddling Dingo Gap to crossing the extensive megaripple field within Hidden Valley. Boxes delineate areas shown in more detail in subsequent figures, with ripple crossing sols shown. B. Elevations color-coded onto a THEMIS daytime visible wavelength image mosaic. Elevation range is ~5.8 km, with red colors corresponding to high and blue to purple colors to low values. Curiosity landed on the plains to the north of Mount Sharp, ~5 km high stack of layered sedimentary rocks. Traverses to the southwest from the landing site were toward these rocks, with an intent of using the onboard instruments to make measurements that would allow reconstruction of the past environments of deposition (Grotzinger et al., 2012). For the HiRISE mosaic BGR colors were assigned to bands located at 0.4 to 0.6, 0.55 to 0.85, and 0.80 to 1.0 micrometers wavelengths. HiRISE is an imaging system on the Mars Reconnaissance Orbiter (McEwen et al., 2007) and THEMIS is a visible to thermal infrared imaging system on the Mars Odyssey Orbiter (Christensen et al., 2004). For reference, Curiosity had traversed ~8.6 km from landing until the sol 710, the last Martian day covered in this paper. Images used in making the mosaics are available through the Planetary Data System.

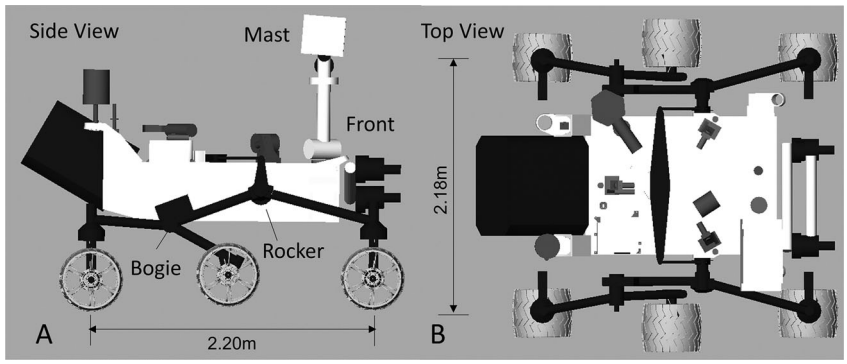

Figure 3. Schematic side (looking at right-hand wheels) and top views of the Curiosity rover showing the dimensions, rocker and bogie suspension pivot points, and the mast.

Engineering data recorded by Curiosity during its drives can be commanded at rates varying from 2 to 64 Hz and include time series of rover tilt vectors (using the onboard inertial maneuvering unit), rocker and bogie suspension angles, wheel turns, and wheel actuator currents. In addition, stereo images are acquired using Hazcam and Navcam cameras. These images are typically acquired at end-of-drive locations to help define paths for next drives.

Table I. Product IDs for Curiosity observations mentioned in this paper. All products are archived in the NASA Planetary Data System (PDS) and may be accessed using the PDS Analyst's Notebook for Curiosity, https://an.rsl.wustl.edu/msl/.

Figure	Product ID
1	0868MH0003900000302175E01_DRCL through 0884MH0003900000302635E01_DRCL
6	CX00530ML0260184F444550544VA
7	N_R000_0539_EDR027CYPTUB0708_DRIVEM1
9	FLB_445258003RADLF0260516FHAZ00216M1 RLB_445258030RADLF0260516RHAZ00306M1
12	CX00672NL0380000F457153643VA
13	RLB_457152495RADLF0380000RHAZ00311M1 FLB_457152435RADLF0380000FHAZ00302M1
15	N_L000_0683_ILT038PER_S_1266_PATH_M1
18	N_L000_0706_ILT040PER_S_0200_DIRCTM1
19	FLB_460433170RADLF0400320FHAZ00322M1 RLB_460432413RADLF0400278RHAZ00322M1

Table II. Threshold settings are shown for megaripple crossings discussed in this paper for maximum rover slip values set for the given sols that, if exceeded, would cause Curiosity to automatically stop its traverse. Also shown are actual maximum slip values observed as determined using visual odometry observations.

Sol	Fast Slip, %	Slow Slip, %	Persistence	Max Slip, %
533	90	70	3	46
535	90	70	3	26
538	60	40	2	51
672	60	40	2	77
683	80	90	4	41
709	60	40	2	78
710	90	70	4	75

Drive distances have ranged from several meters to approximately 100 m, depending on terrain complexity and drive objectives.

3. DATA ANALYSIS, FIELD EXPERIMENTS, AND NUMERICAL MODELING

Analysis of Curiosity-based imaging and engineering data collected during traverses within Gale Crater (Figures 1, 2), experiments with a single-wheel-soil rig (Senatore et al., 2014), field tests with a Curiosity-scale rover (Heverly et al., 2013), and full-scale rover modeling using the Artemis simulation software tool (Zhou et al., 2014) (Figure 4) were all employed to understand the terramechanics associated with Curiosity's megaripple crossings (Figure 2).

For the analysis of drives over the megaripples, slip-corrected traverse distances were derived as a function of rover slip, skid, yaw, pitch, roll, and wheel-drive actuator currents. Relative rover-based elevations were then derived as a function of slip-corrected distances (both for slip and skid, reported as slip-corrected in this paper), using a combination of tilt vectors and suspension angles. The extent of wheel sinkage was estimated using stereo images and associated digital elevation maps covering wheel tracks in regolith and on the megaripples. Wheel currents were also examined, but lack of temperature-dependent calibration

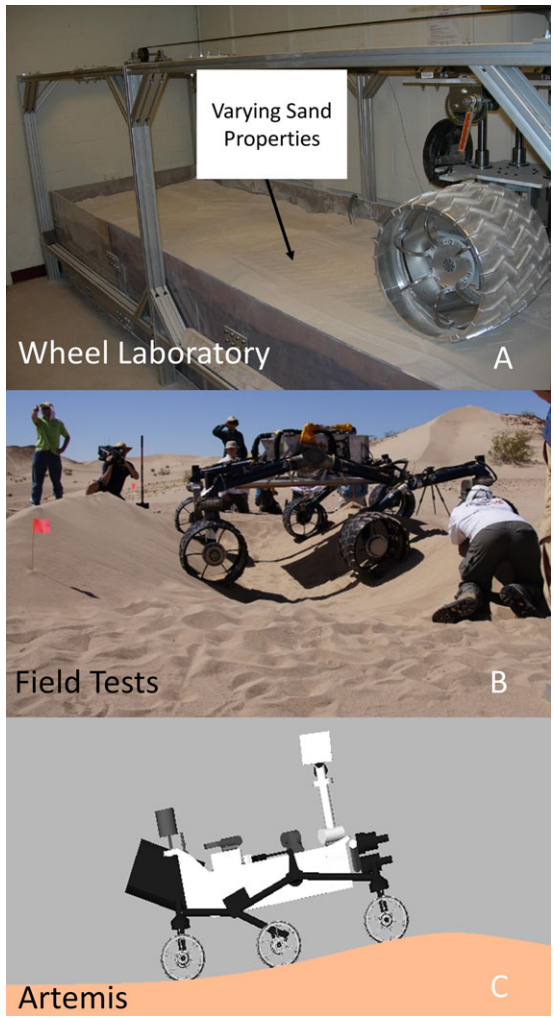

Figure 4. A. View of the laboratory apparatus at MIT where Curiosity single-wheel simulations have been conducted. B. View of the engineering test vehicle, Scarecrow, crossing man-made ripples in the Dumont Dunes, Mojave Desert, California. C. View of an Artemis numerical simulation for the rover driving over realistic topography with spatially varying sand properties. Analysis of Curiosity data, field and laboratory-based experiments, and Artemis simulations were used to understand Curiosity's traverses across megaripples.

data to convert to torque values allowed only qualitative analysis of these data. Slip-corrected distances, elevation, pitch, and slip and skid data presented in this paper are available in digital form from the Planetary Data System (https://an.rsl.wustl.edu/msl/ under Resources).

A spare Curiosity flight wheel was employed at the MIT Robotic Mobility Group terramechanics laboratory to determine wheel sinkage and associated slip as a function of commanded angular velocity, load, tilt, and sand properties (Senatore et al., 2014) (Figure 4A). These experiments allowed us to evaluate single-wheel performance under a variety of situations, including tilted, sand-covered surfaces with and without superimposed ripples. Another set of experiments was conducted using the Scarecrow test rover, a vehicle that has three-eighths the mass of Curiosity to simulate rover loads on Mars. Scarecrow has the same wheels and suspension system as the flight vehicle, and approximately the same center of mass (Figure 4B). Experiments were conducted in the Dumont Dunes, Mojave Desert, California, in May 2012, climbing the face of a dune (Heverly et al., 2013), and again in June 2014, traversing over man-made sand ripples with wavelengths similar to those for encountered Martian megaripples. The latter experiments focused on evaluation of whether Curiosity would encounter mobility problems when crossing megaripples during its traverses in valleys. A detailed evaluation of the ripple crossing experiments at the Dumont Dunes is presented in a Section 8 of this paper.

Artemis is a computationally fast, semiempirical terramechanics software tool for tactical path planning and first-order estimation of terrain properties (Figure 4C) (Zhou et al., 2014). Artemis uses the same commands and produces the same output as engineering data for Curiosity (Arvidson et al., 2014). The model is based on an ADAMS rendition of the rover mechanical system (White et al., 2012), augmented with wheel azimuth and drive actuators in a manner similar to what was done for the Spirit and Opportunity Artemis models (Zhou et al., 2014). Grousers are included in Artemis because they are part of Curiosity's wheels, and they provide additional torque as the wheels move along the surface. Artemis simulates Curiosity's drives using digital terrain maps derived from HiRISE and/or Navcam stereo images, with inclusion of spatially varying regolith or sand properties, or traditional ADAMS contact parameters for surfaces (i.e., bedrock). The wheel-regolith or sand interaction model computes the normal and shear stresses for a set of cells in which the wheels are in contact with the regolith or sand surface, and then integrates over the total contact area using small time steps to determine the torque needed to keep the wheels moving at commanded angular velocities, for example, along specified Ackerman arcs. Normal and shear stresses between the wheels and regolith or sand are modeled using the classical Bekker-Wong-Reece semiempirical terramechanics expressions that describe relationships among normal stress, sinkage, and shear stress as a function of regolith or sand properties for plates (e.g., Wong, 2001, 2012):

$$\sigma = (ck_c + \rho g b k_\phi) \left(\frac{z}{b}\right)^n \tag{2}$$

$$\tau = (c + \sigma n\phi)\left(1 - e^{-\frac{j}{k_x}}\right) \tag{3}$$

where c, k_c, ρ, k_ϕ, and ϕ are the regolith or sand cohesion, cohesion modulus, bulk density, frictional modulus, and angle of internal friction. The parameter k_x is the shear modulus in the longitudinal or drive direction. The other parameters are g, the gravitational acceleration; b, the wheel width; z, the depth of wheel sinkage; n, a scaling parameter; σ, the normal stress; j, the slippage value based on wheel sinkage; and τ, the shear stress between the wheel and regolith or sand. These two basic equations have been converted in Artemis to a wheel cylindrical geometry, as summarized in numerous references (e.g., Tehari, Sandu, Taheri, Pinto, & Gorsich, 2015; Wong, 2001, 2012; Zhou et al., 2014).

The exponent for the pressure-sinkage relationship is used in modified form in Artemis to model to first-order slip-sinkage for cases in which extreme slip leads to regolith or sand excavation beneath the wheel (e.g., Wong, 2001), in addition to compaction:

$$n = n_0 + n_1 \, |slip| \tag{4}$$

Acceleration due to gravity, g, is set as appropriate (3.72 m/s^2 for Mars and 9.80 m/s^2 for Earth) in Artemis to compute forces, and the effects of gravity on regolith or sand self-compression, as shown in the pressure-sinkage relationship shown in Eq. (2) (Nakashima & Kobayashi, 2014; Wong, 2012).

Artemis as a simulation tool was validated using the MIT laboratory single-wheel test-bed data (Senatore et al., 2014) and comparisons to field trials on bedrock and dunes in the Dumont Dunes (Stein et al., 2013). The tool was found to be valid for cases in which wheel sinkage is less than half the wheel diameter, and slip is less than ~60 to 70%. Higher slip values can be modeled, but the empirical equation (Eq. (4)) used to simulate slip-sinkage precludes an in-depth understanding of the interaction mechanics between wheels, regolith or sands.

Iterative Artemis runs allow, by comparison to field-test data or information from Curiosity's traverses, first-order estimation of regolith or sand parameters such as cohesion, angle of internal friction, shear modulus, and the coefficients associated with pressure-sinkage relationships. Simulations are pursued in this paper for crossing the single megaripple straddling Dingo Gap, and the extensive megaripple field in Hidden Valley. The intent is to provide physical insight into how Curiosity interacted with megaripples during its traverses and not to solve for high fidelity, absolute values for sand properties. The latter is difficult given the semiempirical nature of the adopted terramechanics expressions (e.g., Tehari et al., 2015), which

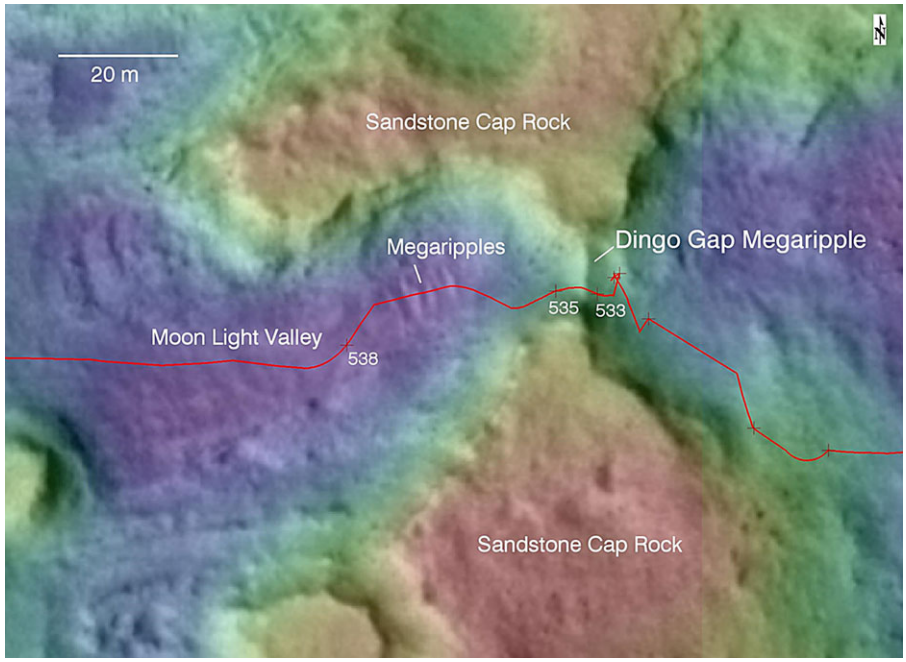

Figure 5. Portion of the HiRISE image mosaic shown in Figure 2 overlain with color-coded elevation data, with a relief of ~7 m from red (high) to blue (low) color-coding. Prior driving over fractured and eroded sandstone-dominated cap rock on the plateaus caused significant wheel damage, thus directing Curiosity through valleys and sandy areas. A single megaripple straddles Dingo Gap, and the rover crossed this feature on sols 533 and 535 to get to Moonlight Valley. The sol 538 drive into the valley included crossing a megaripple field in a local low area. The rover did not drive during intervening sols. Red line shows actual Curiosity traverse path and crosses represent end of drive locations.

were designed to be computationally fast to support tactical path planning.

4. DINGO GAP MEGARIPPLE

Dingo Gap is a narrow pass between two sandstone-covered plateaus. It forms the eastern entrance to Moonlight Valley and other valleys where regolith and windblown sands partially cover the valley floors and thus were judged to be good for minimizing further damage to Curiosity's wheels (Figure 5). Curiosity needed to cross the megaripple that straddles Dingo Gap to enter Moonlight Valley (Figure 6). The megaripple is ~1 m high, with ~7 m wavelength.

The drives over the megaripple were forward (the rover can drive both forward and backward) and accomplished in two parts. First the rover was commanded on sol 533 to ascend the eastern flank, with the front wheels placed near the top of the ridge. On sol 535, Curiosity crossed the megaripple and drove into Moonlight Valley. The drive was biased to the southern side of the megaripple to avoid the center and deepest sands. The ascent also included rotating the front and back wheels 0.082 radians in a counterclockwise direction about their vertical axes to avoid any clockwise yaw toward the center of the ridge. Tracks left by the rover showed wheel sinkage into the sands of up to ~0.05 to 0.07 m in depth (Figure 7), implying that pressure-induced sinkage and associated compaction resistance (e.g., Wong, 2001) would need to be included to understand quantitatively the terramechanics of the drives over the megaripple.

Use of engineering data, coupled with a densely acquired set of visual odometry observations, allowed us to generate plots of rover pitch (tilt along drive direction, which for forward drives is positive when going uphill and negative when going downhill), an elevation profile as sensed by the rover, and slip or skid going up to and then over the megaripple (Figures 8A-B). On ascent, the rover experienced slip, whereas on descent it experienced skid. Left rear wheel (trailing) actuator currents peaked at 1.58 A, and right rear wheel values peaked at 0.93 A during ascent, whereas peak values for the two front wheels (leading) were 0.70 and 0.80 A, respectively. During descent all values were less than 0.45 A. Typical current values for the drive actuators on flat, regolith-covered terrain range from 0.5 to 0.7 A. As noted, the lack of calibration data precludes derivation of torques from the current data, although the trends are indicative of more work needed for the trailing wheels to drive the rover up the megaripple flank.

Artemis was used to simulate this traverse using as input the commands sent to the rover to specify drive waypoints, a digital elevation map generated from Navcam

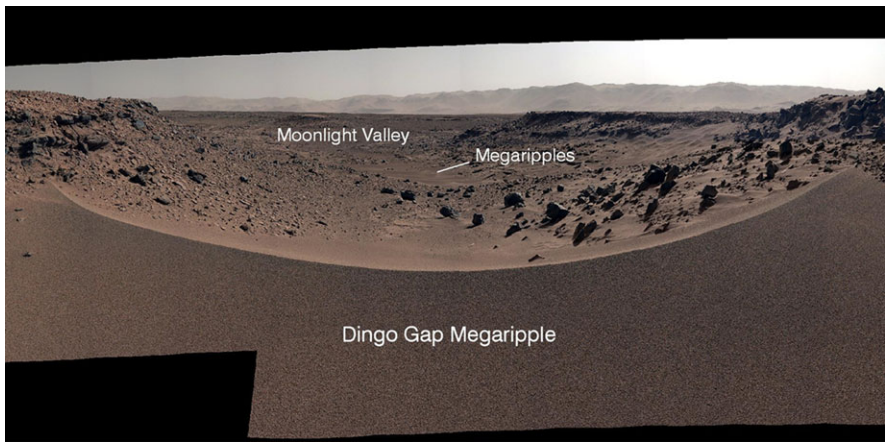

Figure 6. Portion of a Mastcam color image mosaic acquired on sol 530 looking toward the west at the Dingo Gap megaripple and Moonlight Valley. The view also includes the megaripple field crossed on sol 538. Mastcam is the mast-mounted multispectral camera on Curiosity (Bell et al., 2012).

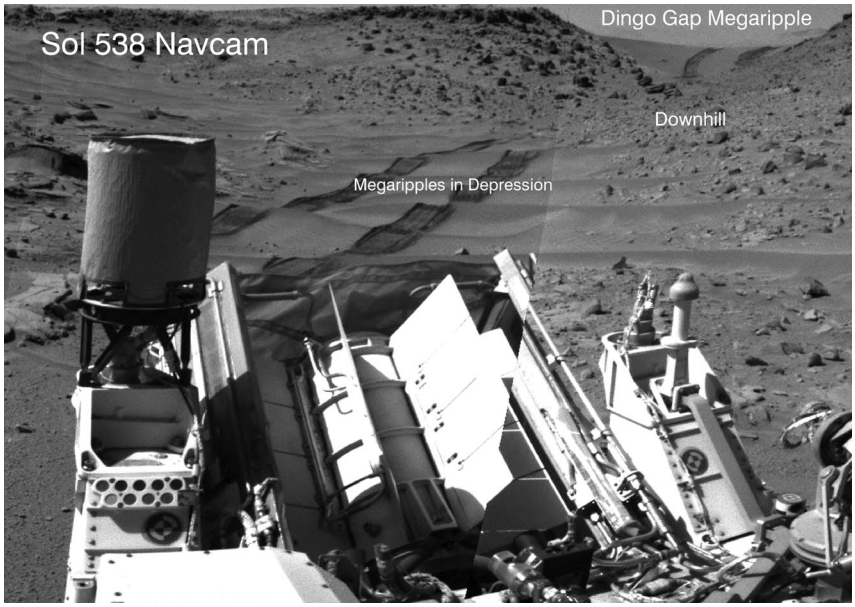

Figure 7. Portion of a Navcam image mosaic taken on sol 539 after crossing the megaripples on sols 533 to 538. Note the dark tracks, which are due to disturbing the overlying dusty surface and exposing underlying basaltic sands.

stereo data, and sand property values that were iterated to have the simulation and Curiosity data conform to one another (Table III, Figures 8C-D). Bulk density, cohesion, and angle of internal friction were held to constant values in the simulations and correspond to slightly cohesive Martian regolith and windblown sands (Sullivan, Anderson, Biesiadecki, Bond, & Stewart, 2011) (Table III). The cohesion modulus was also held constant because the product with the cohesion term is vanishingly small relative to the frictional modulus. The frictional modulus, n_0 and n_1 (Eq. (4)), and the shear modulus were allowed to vary. These free parameters were iteratively adjusted to find minimum sums of squares of differences between simulated and actual slip and skid values, while replicating the wheel sinkage values derived from stereo imaging from Hazcam and Navcam data for the leading and trailing wheels. The simulation replicates increased slip on ascending the megaripple flank as the vehicle pulled against the force of gravity and modest values of compaction resistance. Skid was replicated during the downhill traverse because of the force of gravity, countering compaction resistance associated with wheel sinkage. Inferred sand properties will be compared to results from

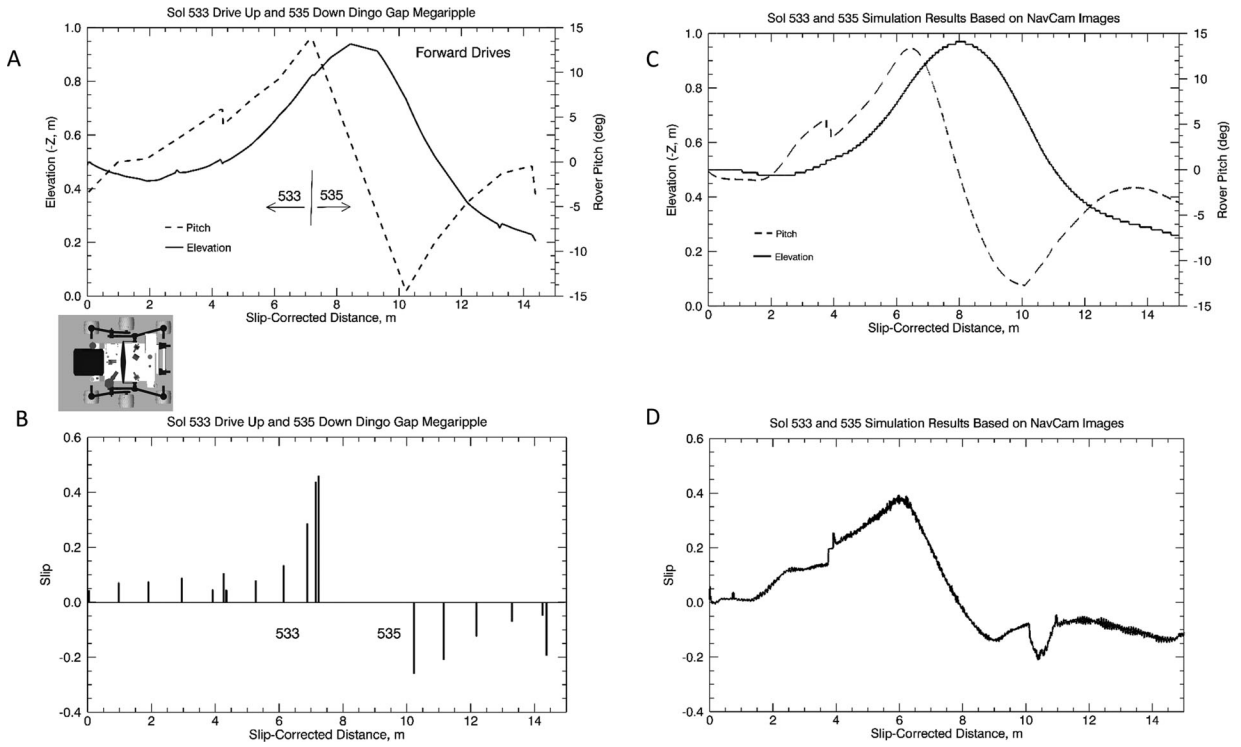

Figure 8. A. Plot of rover-sensed elevation (solid line) and pitch (dashed line) as a function of slip-corrected distance for the sols 533 and 534 traverses across the Dingo Gap megaripple. For these forward drives, positive pitch corresponds to uphill travel, whereas negative pitch corresponds to downhill travel. Rover icon is shown in correct size relative to the traverse distance. The dip in pitch 4.2 m for the Curiosity data is a consequence of a turn in place. B. Plot of slip and skid from discrete stops for visual odometry-based locations as a function of slip-corrected distance. Curiosity shifted from slip to skid as it reached the megaripple crest and started downhill. C. Artemis-based elevation and pitch are shown for the simulated drive over the megaripple. D. Artemis-based slip is shown for the simulated drive over the megaripple. The dip in slip at 11 m distance is an artifact associated with dividing the sol 535 simulation into two segments.

Table III. Numerical values used for megaripples and Dumont Dune sands in Artemis simulations.

	ρ (Kg/m^3)	k_c	k_ϕ	n_0	n_1	C (kPa)	ϕ, deg	k_x (mm)
Dingo Gap Sand Ridge	1300	9	201	1.4	0.2	0.4	30	28
Hidden Valley Ripples	1300	9	86	1.5	0.3	0.1	30	45
Dumont Dunes	1650	9	101	1.5	0.1	0.2	30	32
Dumont Ripples	1650	9	151	1.5	0.1	0.2	30	35

other drives across megaripples and the Dumont Dune field tests in Sections 8 and 9 of this paper.

5. MOONLIGHT VALLEY MEGARIPPLES

On sol 538 Curiosity traversed across a local low region with a megaripple field in Moonlight Valley (Figure 7). Imaging from the Front Hazcams showed slightly cohesive sands, breaking into clods in front of the wheels (Figure 9A). On the basis of measurements from HiRISE, Navcam, and Hazcam data, the megaripples are ~0.1 to 0.15 m high, with wavelengths ranging from ~2 to 3 m. The inter-ripple areas are covered with sand, although it is not possible to determine the depth to bedrock. Wheel sinkage across the ripples was ~0.04 to 0.07 m, based on Rear Hazcam image data (Figure 9B). Wheel grouser and JPL Morse code imprints were well preserved, with consistent compaction and a lack of slip-sinkage (e.g., Wong, 2001). The imprints are consistent with the presence of poorly sorted sands in which silt and clay-sized particles were pushed into voids between sand-sized grains, providing an apparent cohesion and producing high-fidelity imprints (as described

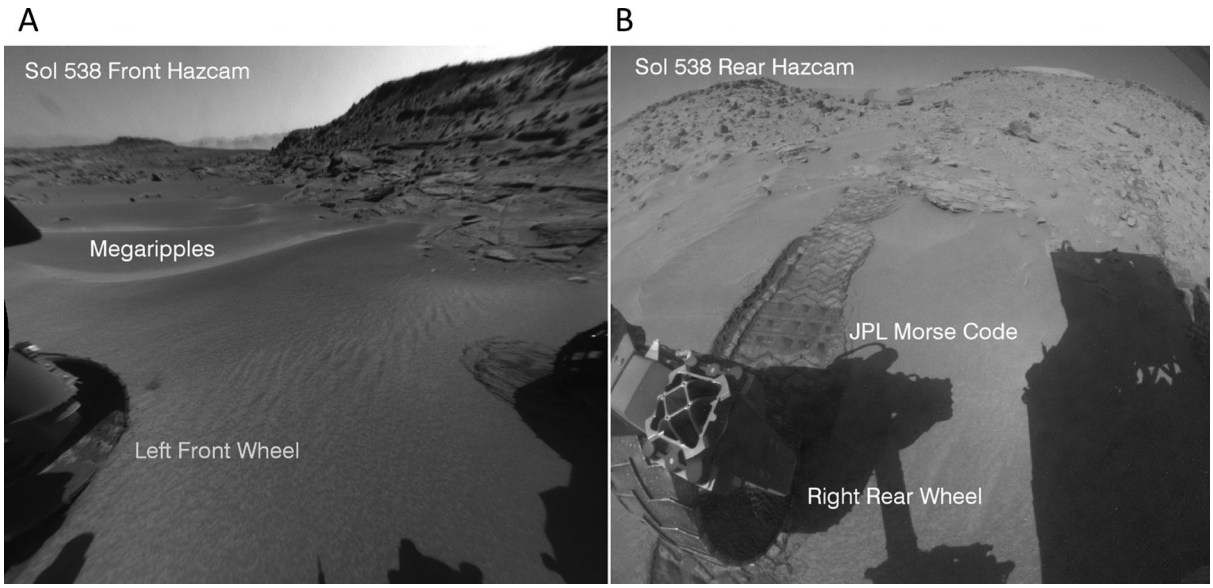

Figure 9. A. Front Hazcam image showing megaripples on sol 538 before traversing over them on this forward drive. B. Rear Hazcam image looking back at ripples traversed. Stereo imaging shows modest wheel sinkage on the right trailing wheel and well-defined wheel tracks, including the imprint of the JPL Morse Code pattern.

in Sullivan et al. (2011) for Spirit and Opportunity Mars rovers).

Examination of engineering data, visual-odometry-based slip and skid, together with wheel sinkage for the sol 538 traverse, shows skid during the downhill drive from Dingo Gap, consistent with a thin regolith cover over bedrock that provided minimal wheel sinkage and compaction resistance (Figure 10). Wheel drive actuator currents were typically less than 0.4 A. High slip values occurred as the vehicle entered the megaripple field, which is located in the topographically lowest part of the traverse. Slip maxima (Table II) occurred in the middle of the megaripple field and decreased as the western edge was traversed. Pitch changes became more closely spaced as the ripples were traversed. Drive actuator ranged up to 0.89 A for the rear (trailing) wheels and 0.71 A for the front wheels (leading) during the megaripple crossing. The overall pattern in the data suggests that a combination increased wheel sinkage into the sands, increased compaction resistance, and a complex ripple topography, may all have been factors that caused the high slip values.

6. MOOSILAUKE VALLEY MEGARIPPLES

A planned 101-m rearward drive on sol 672 began on regolith-covered surfaces on the northwestern side of Moosilauke Valley with a traverse to the southeast, and then south to the deepest part of the valley, crossing an extensive megaripple field (Figure 11). Wheel drive actuator currents were typically less than 0.3 A as the rover traversed downhill. The first set of ripples crossed had wavelengths ranging from ~5 to 10 m, amplitudes of ~0.15 to 0.20 m, and thin sand cover over bedrock between the ripples (Figure 12). Wheel actuator currents while crossing these ripples increased to values as high as 0.5 A. These ripples were crossed without problems, with wheel sinkage of ~0.05 m. The last part of the ripple field was up against a slight incline, ripple crests were closely spaced (~1 to 2 m wavelength, ~0.10 m amplitude), and inter-ripple areas were covered with sand. This was the location in which continued and increasing high drive actuator currents (up to 1.1 A for the front [trailing] wheels) led to an automatic initiation of a visual odometry acquisition, calculation of unacceptably high slip (77%, Table II), and an automatic drive cessation at 82 m distance from the drive starting location. Front Hazcam images show the trailing front right wheel for this backward drive became buried to ~0.15 to 0.17 m depth, whereas the Rear Hazcam images show very little sinkage and provide a good view of the relatively closely spaced ripples (Figure 13). Currents for the two rear wheels (leading) ranged from ~0.5 to 0.8 A. On subsequent sols, the rover was commanded to back out of its sol 672 end position following its tracks, which it did successfully. The traverses were then commanded along the inter-ripple areas with at least partially exposed bedrock surfaces, driving westward and then continuing the long-term route to the southeast.

Plots of elevation and pitch for visual-odometry-corrected distances show the downhill path across the plains to the megaripple field, along with the pitch changes as the rover crossed the relatively widely spaced megaripples

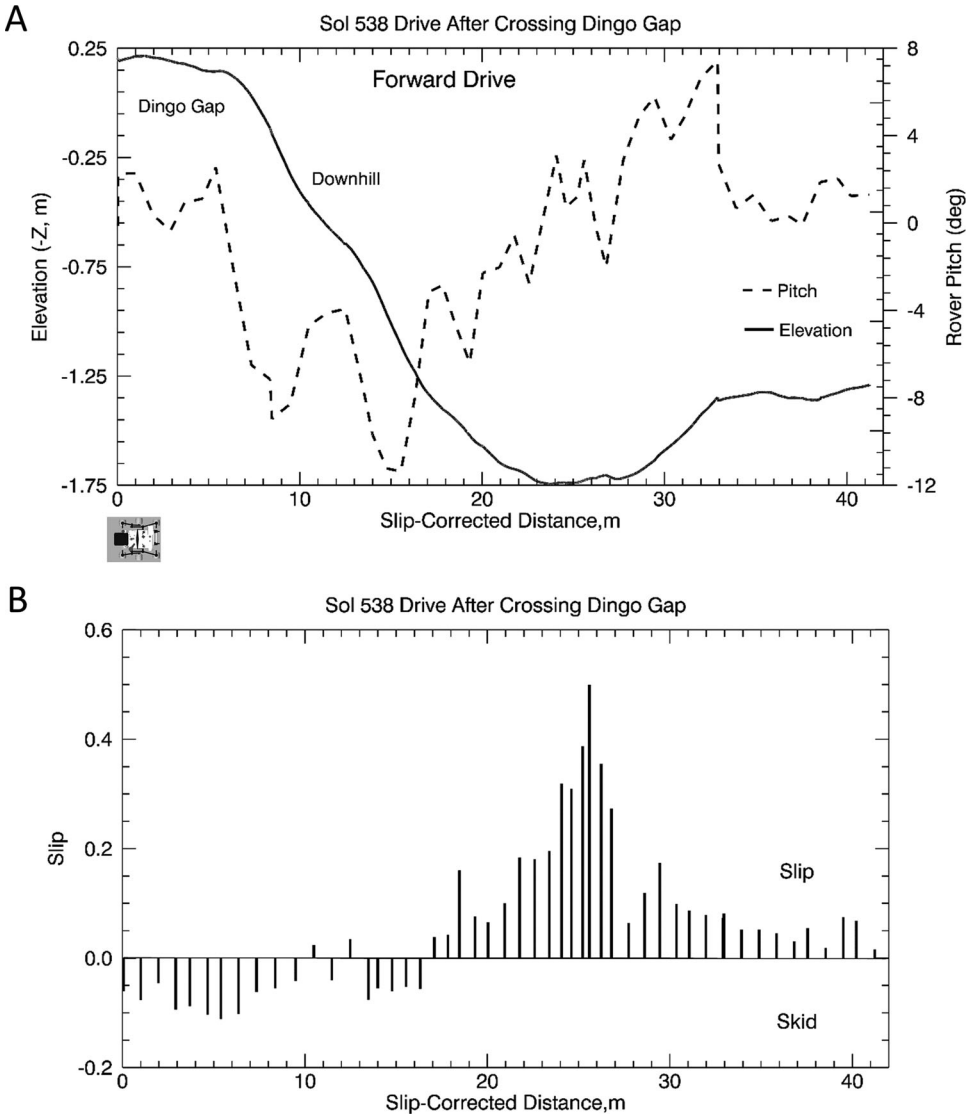

Figure 10. A. Plot of rover-based elevation and pitch as a function of slip-corrected distance for the sol 538 drive into Moonlight Valley, including crossing the megaripple field. Rover icon is shown in correct size relative to the traverse distance. For this forward drive, positive pitch corresponds to uphill travel, whereas negative pitch corresponds to downhill travel. B. Plot of slip and skid as a function of slip-corrected distance. Curiosity shifted from skid to slip as it started downhill on regolith-covered surfaces and encountered a local low area with ripples. Slip peaked in the middle of the ripple field.

(Figure 14A). Pitch on this backward drive shows uphill and then downhill motions as the rover first ascended and then descended the flanks of these ripples. Visual odometry data were only occasionally collected but do show modest skid going downhill on the plains, followed by slip in the ripple field (Figure 14B).

After crossing the megaripple straddling Dingo Gap, and the megaripple fields on sols 538 and 672, it was considered important to conduct a controlled experiment with a high density of visual odometry observations and associated engineering data while crossing a single megaripple in Moosilauke Valley. The reason for choosing a single ripple was to minimize the number of variables and to evaluate the magnitude of wheel sinkage, slip on ripple ascent, and skid on descent. A single ~6 m wavelength and ~0.4 m amplitude ripple was chosen for a frontward crossing on sol 683 and the experiment was successful (Figures 15, 16). Both slip and skid occurred, values were not particularly high (Table II), and reminiscent of the Dingo Gap megaripple crossing. The rear wheel (trailing) drive actuator current

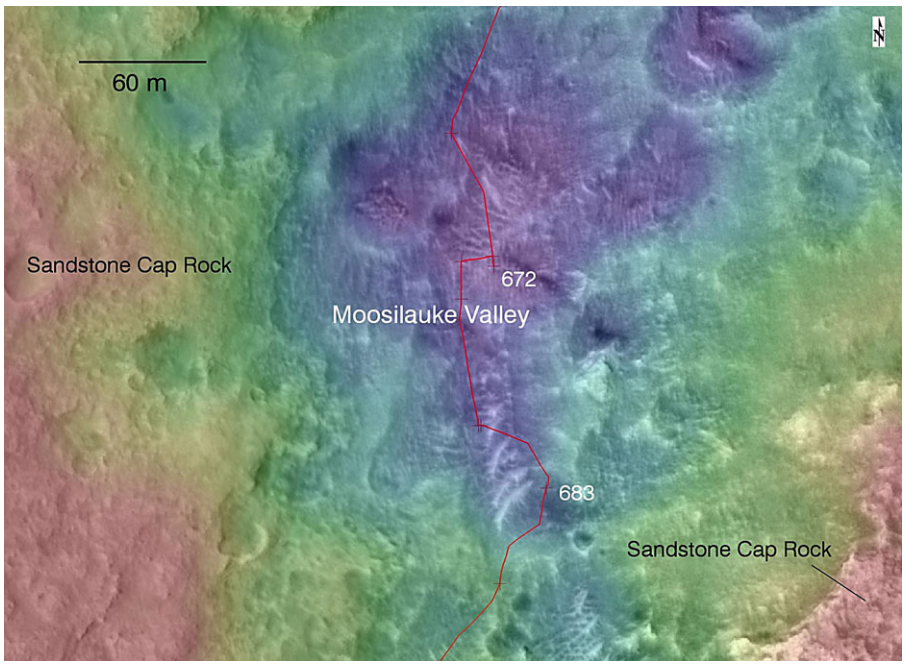

Figure 11. Portion of a HiRISE image mosaic shown in Figure 2 overlain with color-coded elevation data, with a relief of ~11 m from high (red) associated with sandstone-covered plateaus (cap rock) to low (blue and purple) valleys. Megaripple fields were crossed on sols 672 and 683. The sol 683 single megaripple crossing was an experiment in which a dense suite of engineering and image data were acquired to better understand ripple crossing dynamics. Red line shows actual Curiosity traverse path.

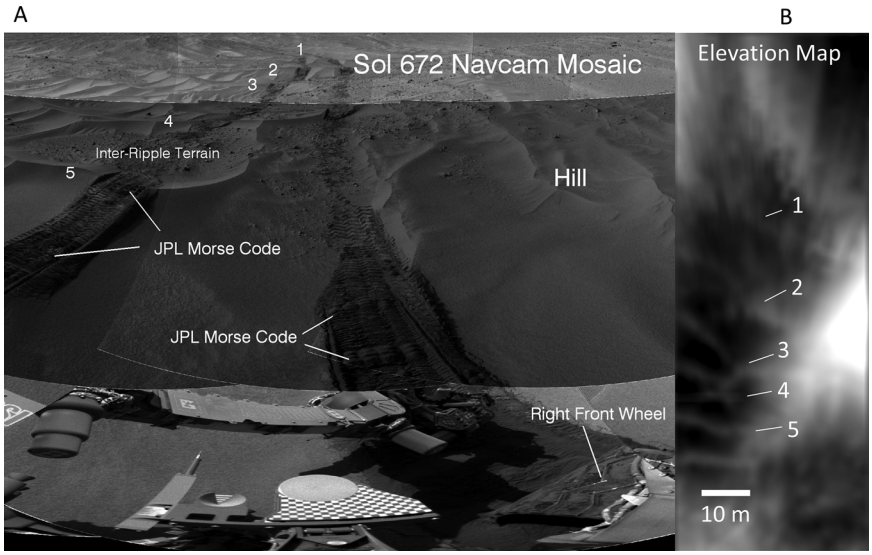

Figure 12. A. Portion of the sol 672 Navcam mosaic showing megaripples crossed before a 77% slip value led to an automatic cessation of this rearward traverse. B. Topographic map generated from the Navcam stereo image coverage, with bright areas corresponding to higher regions. Relief in the Navcam-based map is ~0.5 m. Ripple features are correlated between the image and map using a set of numbers. As Curiosity approached high slip values the wheel track imprints became disrupted and the JPL Morse code patterns imprinted into the sand became closer together.

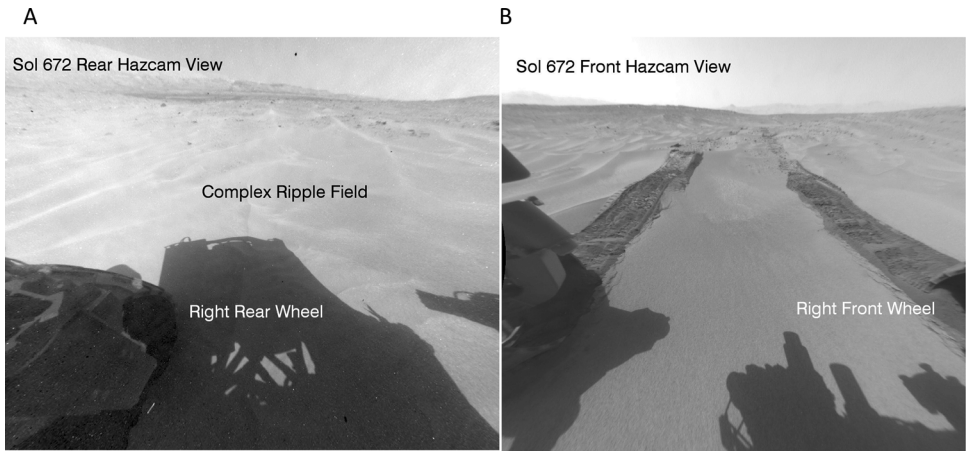

Figure 13. A. Sol 672 Rear Hazcam image showing little wheel sinkage for the leading right wheel on this backward drive. B. Front Hazcam image showing wheel sinkage for the right front wheel.

peaked at 1.42 A during ascent, with values less than 0.4 A for the front wheel (leading) actuators. Wheel currents during ripple descent averaged ~0.3 A. Wheel sinkage at the crest of the ripple, based on examination of Rear Hazcam image data, was ~0.03 to 0.07 m. It is likely that the trailing wheels, while helping get the rover across the ripple crest, did not encounter deep sand. Rather, those wheels were on thin sand covering bedrock surfaces, and maintained traction until the leading wheels crested and the rover began the descent. Results showed that Curiosity was capable of traversing across single megaripples without excessive slip, in the same way that occurred for the Dingo Gap megaripple, and the several widely spaced megaripples encountered on sol 672 in the northern portion of that ripple field.

7. HIDDEN VALLEY MEGARIPPLES

On sol 706 Curiosity reached the entrance to Hidden Valley and acquired extensive imaging data to provide terrain information that would allow an assessment as to whether the extensive megaripple field located on the valley floor would be traversable (Figures 17, 18). This field has megaripples with wavelengths of ~2 to 3 m and amplitudes of ~0.15 to 0.20 m, with smaller ripples in sand-covered inter-ripple regions. The preferred path would have been along the southern margin of the megaripple field (nicknamed the "shoreline"), staying on the boundary between the megaripples and the southern slope extending downward from the sandstone bedrock on the southern plateau. To get there, the rover was commanded to traverse across the megaripple field because large talus blocks precluded starting the drive on the western portion of the "shoreline" (Figures 17, 18).

Driving backward through this complex and deep megaripple field proved to be problematic, and the vehicle sensed continued high motor currents that initiated a visual odometry session, with a high slip estimation while in the middle of the ripple field, and driving in a slight (~3°) uphill direction (Figures 18, 19). The high slip values led to an automatic drive cessation (Table II). Wheel drive actuator currents at the start of the drive ranged from 0.2 to 0.55 A, with the rear wheel (leading) values ending at approximately 0.5 A. The trailing wheel drive actuators at the end of the drive had values that ranged from 0.9 to 1.05 A. Imaging of the wheels and tracks showed deep sinkage of the trailing wheels, and a change from detailed wheel imprints (compaction-dominated) to disrupted features, consistent with disrupting sands in a slip-sinkage mode (Figure 19). Trailing wheels were buried to ~0.15 to 0.18 m. Leading wheels did not show appreciable sinkage, a situation reminiscent of the sol 672 ripple crossing.

Artemis was used to simulate the drive into Hidden Valley, using a digital elevation map generated from Navcam stereo data and the drive commands used for the sol 709 traverse across the megaripple field (Figure 20). The same sand properties as used for Dingo Gap, with the addition of cohesion, were adjusted to match slip values observed by Curiosity and the trailing wheel sinkages at the end of the drive (Figures 19C-D; Table III). Cohesion was added because images of the ripples suggested less cloddy behavior when disturbed, relative to the Dingo Gap megaripple. The simulation shows modest skid on the downhill portion of the drive, but generally replicates the slip patterns observed by Curiosity (Figure 20). As a comparison, a simulation using Dingo Gap megaripple sand properties (Table III) was also conducted using the same elevation data. Slip values for the Dingo Gap sand properties did not exceed thresholds for drive cessation. Differences between these two simulations suggest, within the limitations of the Artemis modeling regime, that the sands in Hidden Valley are more compressible (thus with more compaction resistance) than those encountered while crossing the megaripple straddling

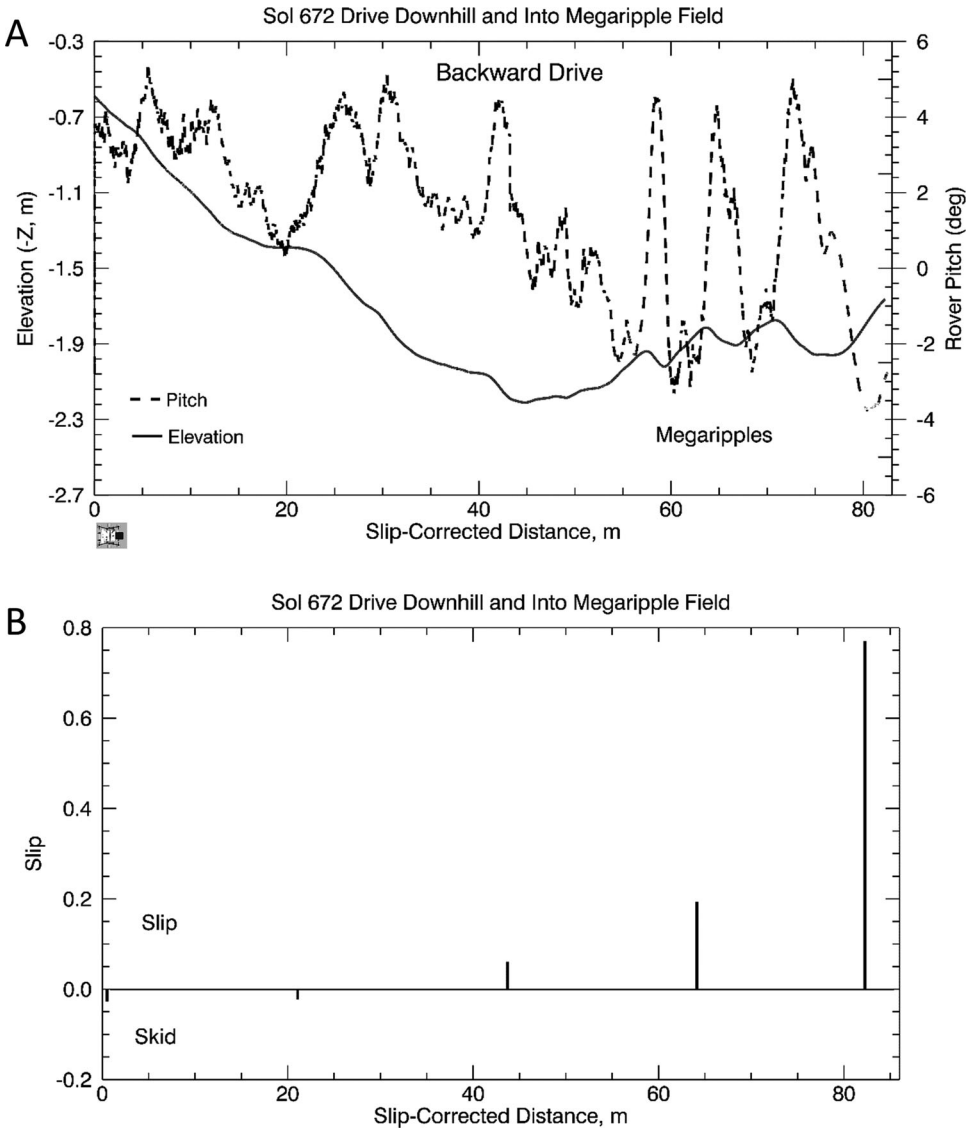

Figure 14. A. Plots of rover-based elevation and pitch as a function of slip-corrected distance for the sol 672 drive. B. Plot of slip as a function of slip-corrected distance. Only a few slip values were planned and acquired during the traverse. Onboard detection of anomalously high drive actuator currents automatically launched a visual odometry measurement to evaluate slip. The high value detected was above the threshold setting (Table II), and the rover stopped its traverse.

Dingo Gap. Further, the shear coefficient for the shear stress slip relationship indicates that the Hidden Valley sands tend to have more slip for given normal and shear stresses (Table III).

On sol 710 the rover was commanded to reverse its path back to the entrance to Hidden Valley, and analysis of telemetry showed high slip values as the rover traversed through the sands in an uphill direction (Figure 21). Wheel drive actuator currents ranged from 0.45 to 1.0 A, with higher values for the rear (trailing) wheels. The drive was planned to traverse along the tracks made during the sol 709 drive, thereby taking advantage of the compressed sand, with less sinkage and associated compaction resistance. The rover yawed out of the tracks. The increased currents and slip are interpreted to be due to a combination of working against gravity while driving uphill and increased compaction resistance as new sands were compressed by wheel loads. Continued high currents again led to an automatic drive cessation. Two drives later the rover reached the entrance to Hidden Valley.

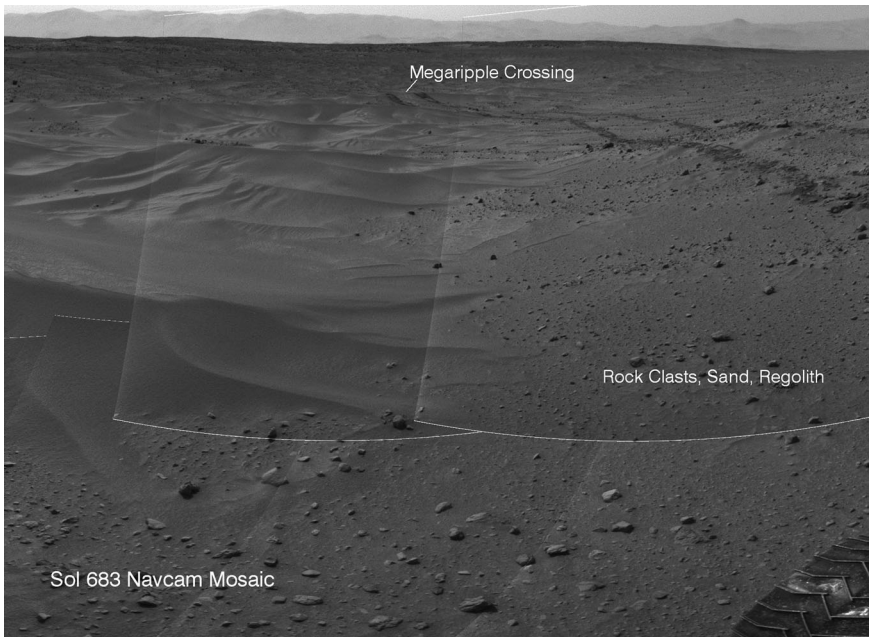

Figure 15. Portion of a sol 683 Navcam mosaic looking back at the megaripple traversed as part of a ripple crossing experiment in which a dense array of engineering data was collected. The majority of the traverse was across regolith-covered plains strewn with rocks.

A decision was made after the Hidden Valley drives to avoid extensive megaripple fields and to drive in valleys covered by regolith, relatively thin windblown sand covers, and single megaripples. Drives were also accomplished when needed on the sandstone-dominated plateau surfaces, biased toward local low areas where thin sand deposits would cushion the wheels from further punctures and tears from sharp rocks. For example, after exiting Hidden Valley, Curiosity was commanded to drive to the north and west over plateau surfaces (Figure 17). This approach proved to be successful and Curiosity reached the base of Mount Sharp in Pahrump Hills on sol 753 to conduct an extensive set of scientific measurements on the exposed fluvial-lacustrine rock strata (Vasavada et al., 2015).

8. CURIOSITY DATA COMPARED TO SCARECROW EXPERIMENTS ON DUNES AND ARTIFICIAL RIPPLES AT THE DUMONT DUNE FIELD

Curiosity telemetry data show that slip values greater than ~50%, along with enhanced trailing wheel drive actuator currents, occurred during crossing the extensive megaripple fields on sol 538, 672, 709, and 710 (Table II). A plot of slip as a function of rover tilt shows a wide range of slip values for these crossings (Figure 22). However, the traverses across the Dingo Gap megaripple, the sol 683 megaripple, and drives across valley floors with bedrock partially covered by regolith or thin covers of windblown sand, showed the more classic increase in slip with increasing tilt, and skid while driving downhill (Figure 22). The classic pattern of increased slip with increased tilt includes results from field tests using the Scarecrow rover in 2012 generated while driving up the flank of a large dune in the Dumont Dunes (Heverly et al., 2013). Overall results suggest that the material properties of sands in deep, extensive megaripple fields, together with megaripple geometries, were both involved in generation of high wheel sinkage, increased actuator currents for the trailing wheels, and high slip values.

To better understand how Curiosity interacted with megaripples during its crossings Scarecrow was redeployed to the Dumont Dunes in June 2014. Artificial ripples (not megaripples because coarse-grained monolayer was not present) were constructed with approximately the same wavelengths as found for the megaripples Curiosity crossed, and was expected to cross, if and when further crossings were planned (Figure 23). Amplitudes were purposely set higher than found for the megaripple fields in order to provide worst-case scenarios. Scarecrow was driven forward in the morning and then backward in the afternoon over these ripples, and slip was monitored on a continuous basis using the same monitoring systems used during the 2012 tests (Heverly et al., 2013). After each run, the ripples were rebuilt using shovels, with a noticeable shift to steeper ripples by the afternoon backward runs. Slip and skid as a function of rover pitch show a wide range of slip values, even though wheel sinkage visually determined was

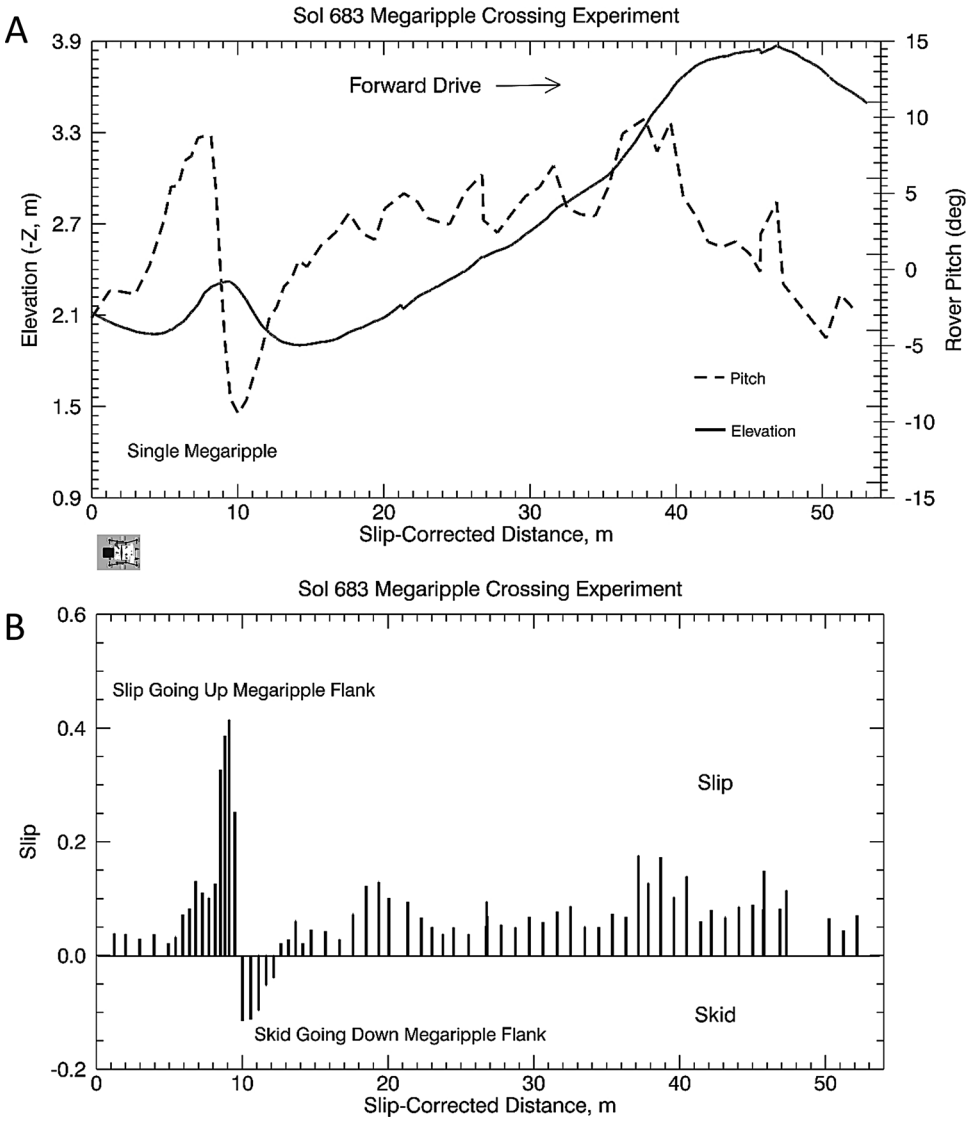

Figure 16. A. Plot of rover-based elevation and pitch for the sol 683 drive, in which pitch changes ascending and descending the single megaripple are evident over the first 15 m of the traverse. B. Plot of slip and skid as a function of slip-corrected distance. Note the transition from slip to skid as Curiosity crested the megaripple.

typically less than ~0.05 m (Figure 24A). Slip approached ~95% in some cases, for both forward and backward drives. The leading wheels typically excavated the ripple crests until the pitch decreased enough for the rover to continue its drive. The pattern of slip as a function of pitch was much more complex than the relatively simple increase in slip with increasing pitch associated with climbing the flanks of the Dumont Dunes (Figure 24A), and reminiscent of the pattern observed while Curiosity traversed extensive, deep megaripple fields on sols 538, 672, 709, and 710 (Figure 22).

9. SINGLE-WHEEL EXPERIMENTS AND ARTEMIS SIMULATIONS TRAVERSING ACROSS DUMONT DUNE RIPPLES

To further understand the underlying causes of high slip situations while crossing megaripples, single-wheel tests using the MIT wheel-soil rig with a spare Curiosity wheel (details of the rig set-up and sand properties in Senatore et al. (2014)) were run with tilted, sand-covered surfaces, with and without superimposed sand ripples. Ripple amplitudes were set to be comparable to those crossed by Curiosity. Results showed that increasing slope on a tilted,

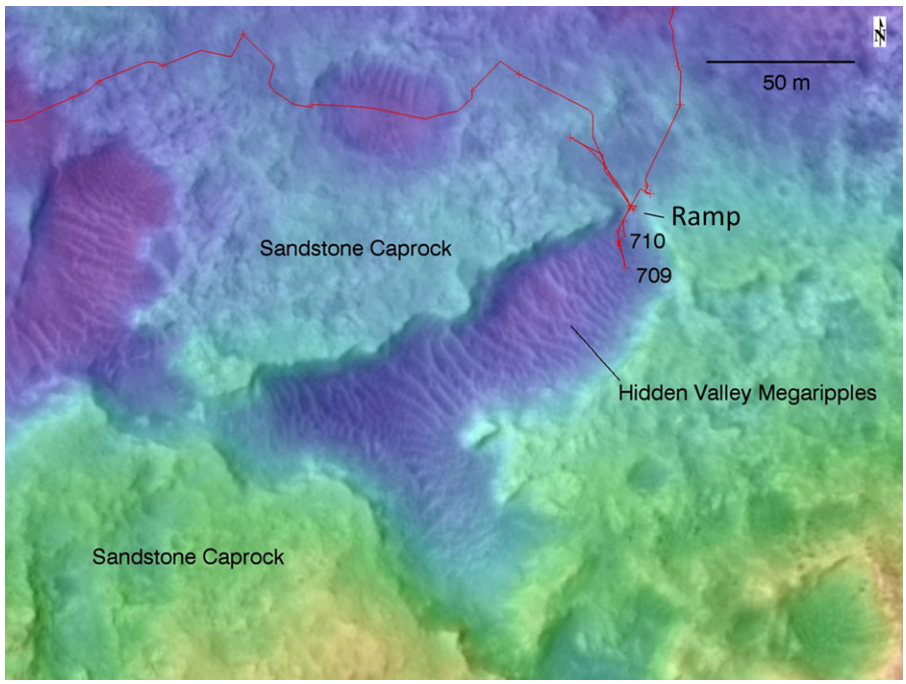

Figure 17. Portion of a HiRISE image mosaic shown in Figure 2 overlain with color-coded elevation data, and centered over Hidden Valley, with a relief of ~10 m from high (red) associated with sandstone-covered cap rock plateaus, to low (blue and purple) values in Hidden Valley. The sol 709 backwards drive was an attempt to cross the megaripple field in Hidden Valley and led to an automatic drive cessation when high slip values were measured. Red line shows actual Curiosity traverse path.

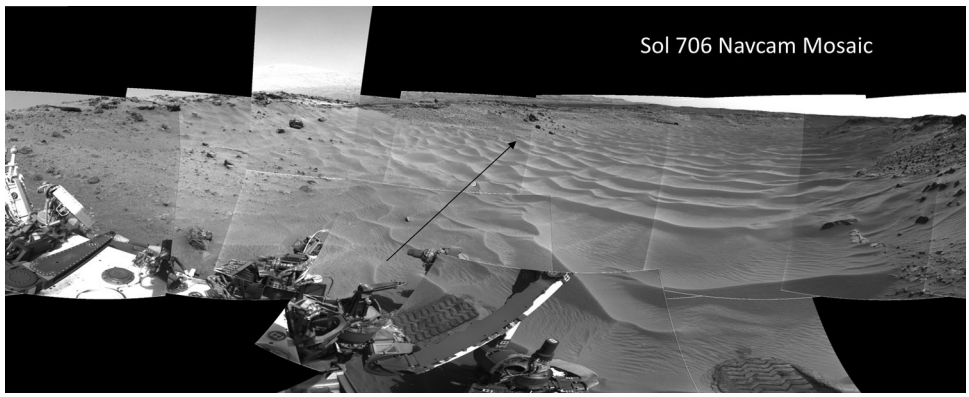

Figure 18. Portion of a sol 706 Navcam mosaic looking into the megaripple field in Hidden Valley, with the approximate sol 709 drive path across the ripple field shown. The drive was planned to cross the ripple field to get to the southern "shoreline" and to then continue along the southern valley wall.

sand-covered surface produced a slip vs pitch curve much like the one found for climbing the Dumont Dune flank. On the other hand, placing ~0.10 m high ripple on the tilted surface increased slip significantly, and a working hypothesis was that the increased pitch of the local surface moved the interactions further along the slip-pitch curve.

The single-wheel experiments were exploratory and hinted at one of the reasons for increased slip when crossing megaripple fields. However, the complex slip, skid, and tilt patterns evident for both the Dumont ripple and Mars megaripple crossings suggested that a more complicated explanation was needed. To that end, a series of Artemis simulations were conducted across simulated Dumont Dunes ripples of varying amplitudes. These runs produced slip, skid, and pitch patterns similar to those evident for the Scarecrow ripple and Curiosity megaripple crossings

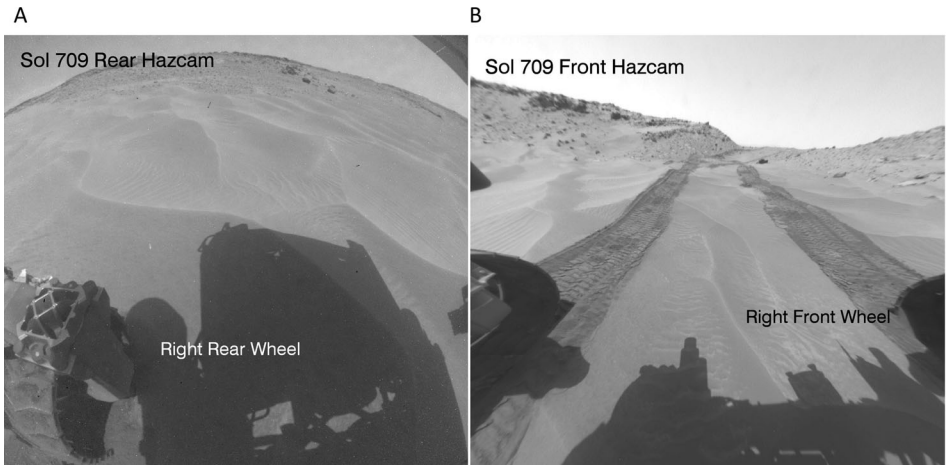

Figure 19. A. Sol 709 Rear Hazcam image showing little wheel sinkage for right rear (leading) wheel during the traverse into the megaripple field in Hidden Valley. Also note the lack of bedrock exposures in the inter-ripple areas. B. Sol 709 Front Hazcam image looking back at tracks produced during entry into Hidden Valley. Note track imprint disruptions and deeply buried right front trailing wheel.

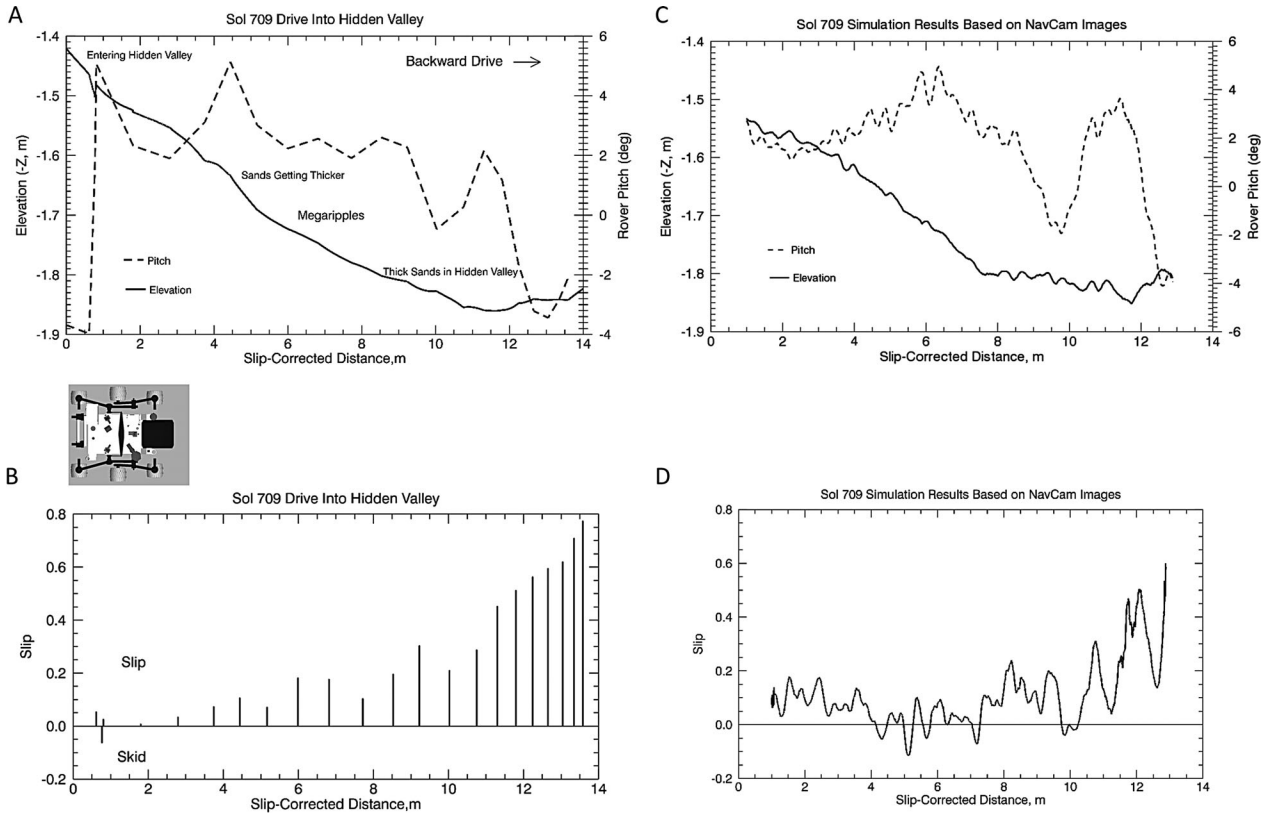

Figure 20. A. Plot of rover-based elevation and pitch as a function of slip-corrected distance for the sol 709 backward drive in Hidden Valley. B. Plot of rover-based elevation as a function of slip. While driving downhill slip as opposed to skid dominated the drive because of the retarding effects of sandy megaripples, that is, increased wheel sinkage and associated compaction resistance. The drive was automatically stopped when slip exceeded the threshold value (Table II). C. Plot from Artemis simulation of rover-based elevation and pitch as a function of slip-corrected distance. D. Plot from Artemis simulation of slip and skid as a function of slip-corrected distance.

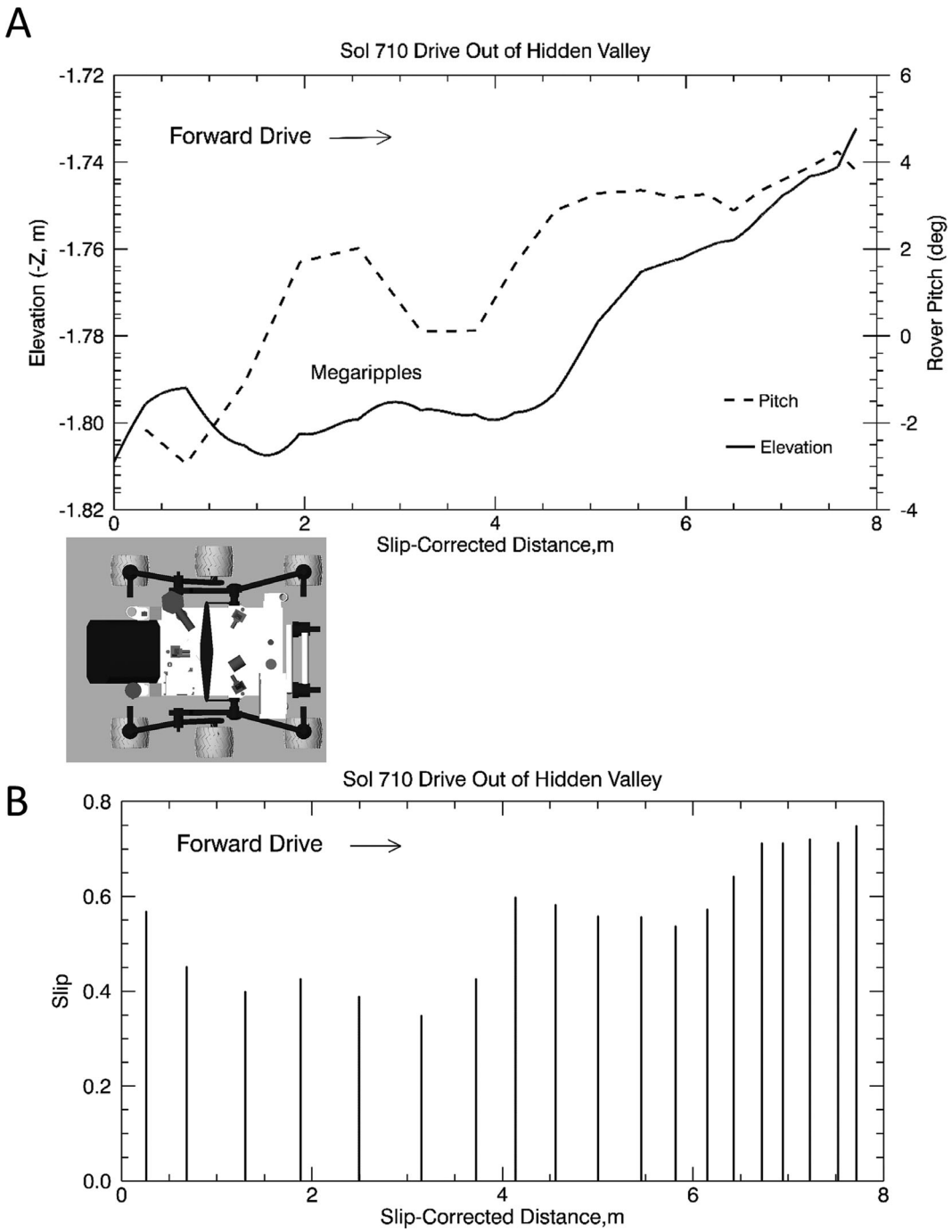

Figure 21. A. Plots of elevation, pitch for the sol 710 drive out of Hidden Valley. B. Slip as a function of slip-corrected distance. High slip values occurred during this uphill drive over ripples, both because of the downhill pull due to gravity and yawing out of the sol 709 tracks.

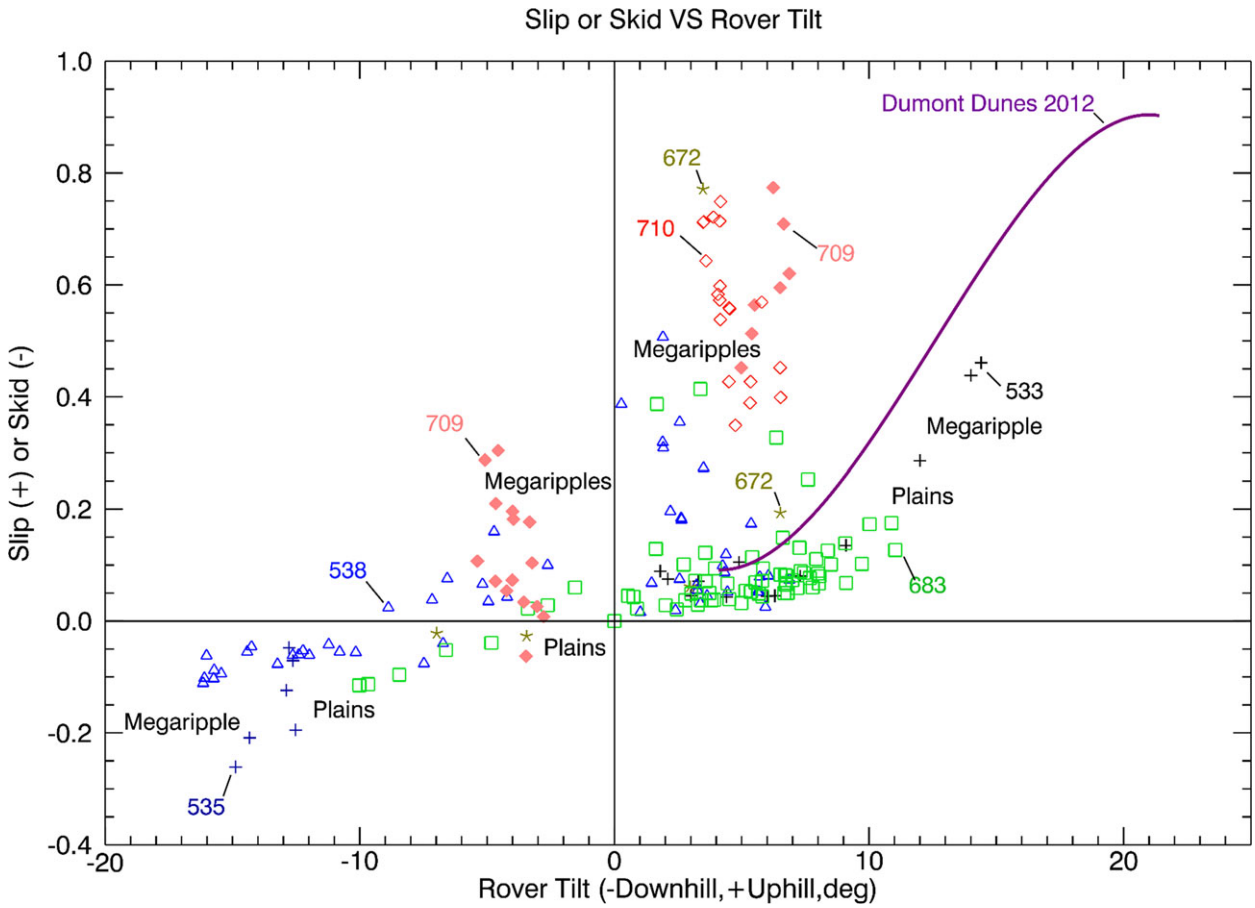

Figure 22. Plot of slip, skid, and rover tilt for the Curiosity data presented in this paper, along with an uphill traverse during the 2012 field tests on a Dumont Dunes dune face. Tilt rather than pitch is used for the abscissa because slip and skid did not always occur along the pitch direction. Note that the regolith-covered plains and the Dingo Gap megaripple data occupy the lower portion of the data swarm, whereas the crossings of extensive megaripple fields have higher slip values and are more variable. Data are color-coded by sol traversed and by symbols. Dumont data are approximated by a polynomial fit to data reported in Heverly et al. (2013).

(Figure 24B). For both backward and forward drives, the high slip situations were associated with poses in which the rover needed to increase wheel drive actuator currents (and thus torque) to propel one or more wheels up and over ripple flanks and/or crests (Figures 25 and 26). Simulated wheel sinkage patterns are complex and proportional to static loads associated with specific poses as the rover traversed across the ripples (Figures 25 and 26). Skid occurred in the Artemis runs when one or more wheels were descending the ripple flanks. More skid is evident in the Artemis models than found for the Dumont and Mars ripple data. This is interpreted to be associated with an observation during Dumont Dune ripple crossings in which leading wheels excavated the ripple crests until the rover was able to continue its drives, thereby negating the skid portion of the drives. A similar phenomenon may have occurred during the Moosilauke Valley and Hidden Valley megaripple crossings. This phenomenon was difficult to reproduce using Artemis. Overall, the similarities between megaripple and ripple crossings also demonstrate that the coarse-grained monolayer that distinguishes megaripples from ripples does not influence the terramechanics associated with crossing megaripples.

Artemis was also run using its contact model in which the surfaces were assumed to be nondeformable and characterized by static and dynamic coefficients of friction and transition velocities used for simulations of an Opportunity rover drive over bedrock on the Endurance Crater rim (Zhou et al., 2014). Results show the same patterns of slip and skid as a function of rover pitch, with more abrupt transitions that are smoothed out by use of the deformable sand model shown in Figures 25 and 26. Thus, both the geometry

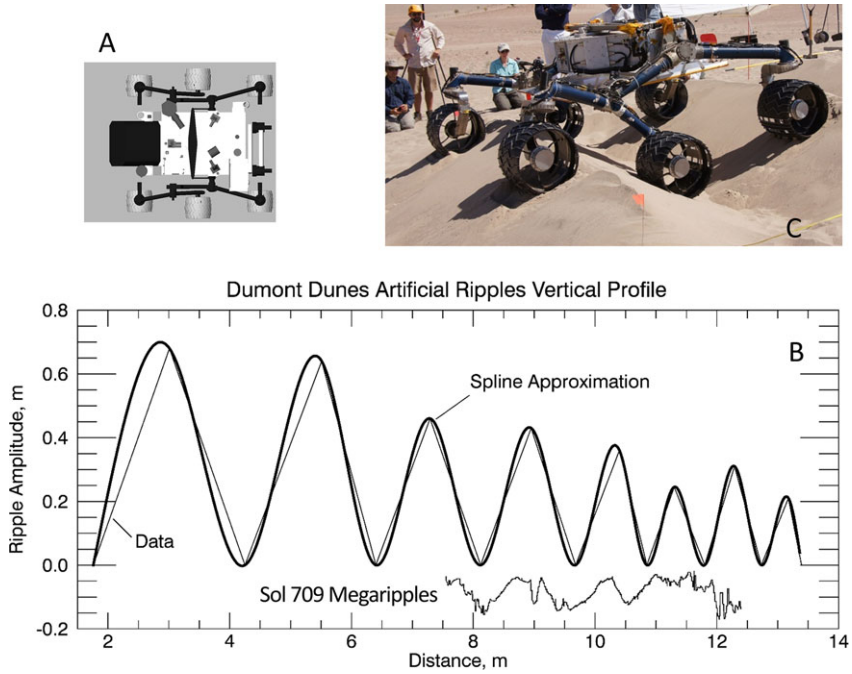

Figure 23. A. Rover icon scaled to the ripple distance for artificial ripples made in the Dumont Dunes. B. Plot of a topographic profile for the manmade ripples, fit with a cubic spline. Plot also shows a topographic profile for the Hidden Valley megaripples generated from topographic data extracted from the sol 709 Navcam stereo images. Note that the Hidden Valley ripples have approximately the same wavelengths but much smaller amplitudes as compared to the Dumont ripples. C. Scarecrow rover is shown during one of its traverses across the ripples.

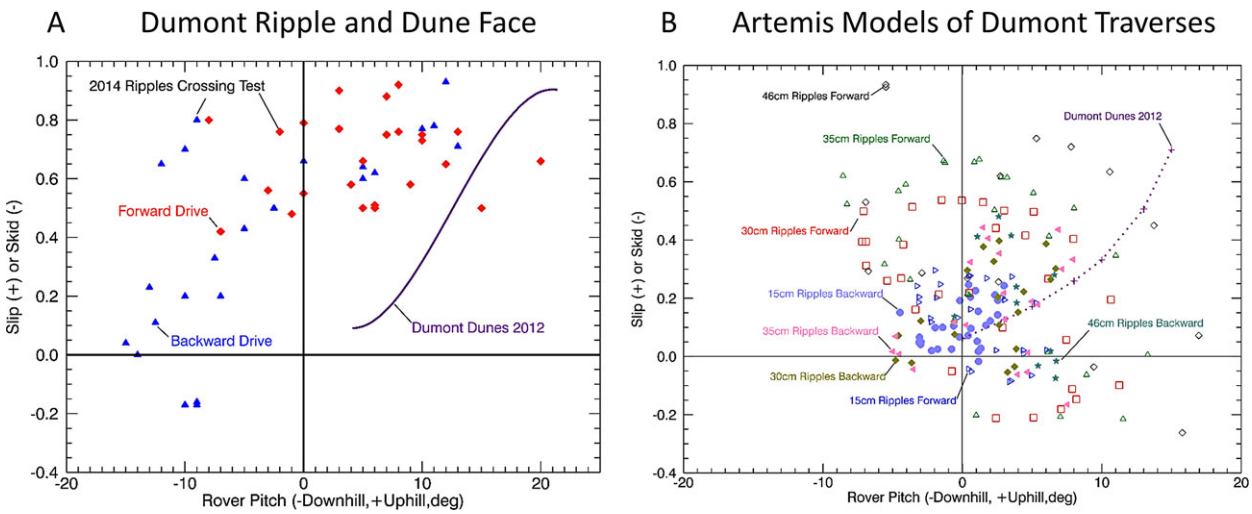

Figure 24. A. Plot of slip and skid as a function of pitch for forward and backward Scarecrow drives across the Dumont ripples, with ripple amplitudes ranging from 0.35 to 0.40 m and a mean wavelength of 1.73 m. B. Plot of slip, skid, as a function of pitch for Artemis simulations across ripples of constant 1.73 m wavelength and varying amplitudes. Sand properties for the dune face ascent were based on Zhou et al. (2014), whereas the cohesion, frictional modulus, shear modulus, n_0 and n_1 were adjusted to match slip and sinkage values observed during Dumont Dune ripple crossings (Table III).

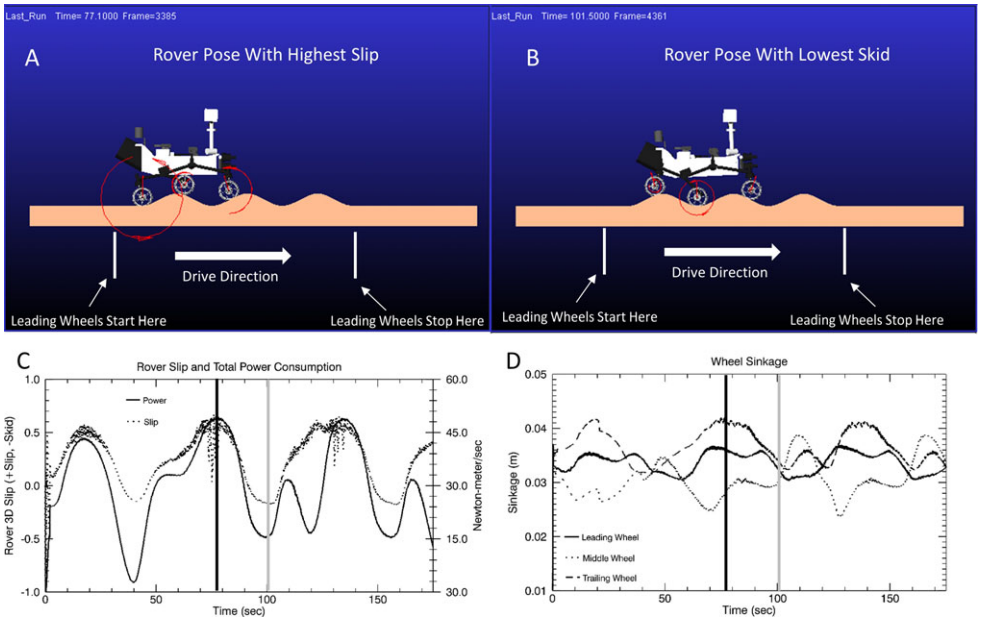

Figure 25. A. Artemis-based rover pose for maximum slip for a forward drive over 1.73 m wavelength and 0.30 m high ripples. B. Artemis-based rover pose for maximum skid for a forward drive over 1.73 m wavelength and 0.30 m high ripples. C. Slip, skid, and total wheel drive actuator power consumption are plotted as a function of simulation time. Dark vertical line is shown for the time for which the rover pose is shown in Figure 25A (slip). Gray line is shown for the pose shown in Figure 25B (skid). D. Wheel sinkage values are plotted as a function of simulation time, with the same vertical lines as shown in Figure 25C. Sand parameters were used from Table III for the Dumont ripples.

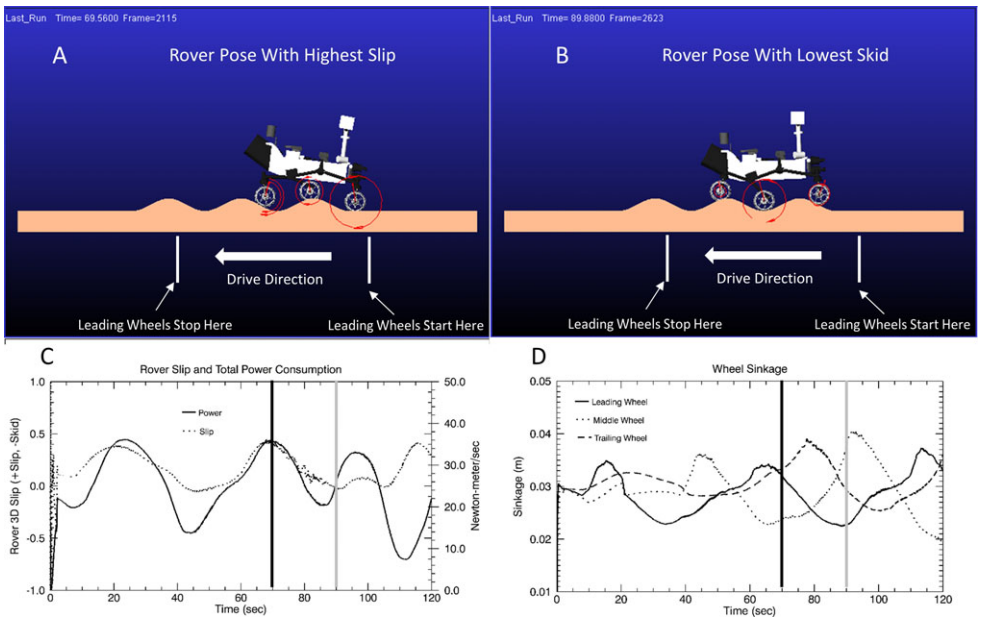

Figure 26. A. Artemis-based rover pose for maximum slip for a backward drive over 1.73 m wavelength and 0.30 m high ripples. B. Artemis-based rover pose for maximum skid for a backward drive over 1.73 m wavelength and 0.30 m high ripples. C. Slip, skid, and total wheel drive actuator power consumption are plotted as a function of simulation time. Dark vertical line is shown for the time for which the rover pose is shown in Figure 26A (slip). Gray line is shown for the pose shown in Figure 26B (skid). D. Wheel sinkage values are plotted as a function of simulation time, with the same vertical lines as shown in Figure 25C. Sand parameters were used from Table III for the Dumont ripples.

of the megaripples and sand material properties are interpreted to have influenced the terramechanics of Curiosity's megaripple crossings.

10. CONCLUSIONS AND IMPLICATIONS

This paper examined the ability of the Curiosity rover to traverse across windblown, sand-dominated megaripples, including high slip and wheel sinkage events associated with crossing megaripple fields that are extensive and deep enough to cover the underlying bedrock and regolith completely. Crossing bedrock, regolith-covered bedrock, and single megaripples, including one straddling Dingo Gap, showed the classic slip as a function of tilt while driving uphill and skid as a function of tilt while driving downhill. Traversing extensive megaripple fields, with ripple crests separated by wavelengths comparable to the front-to-back wheel distances, produced complex slip as a function of rover tilt, with extreme slip values up to 77%, and trailing wheel sinkages up to ~0.15 to 0.17 m or ~30% of the wheel diameter. Single-wheel tests, experiments conducted with a three-eighths mass rover over artificial ripples at the Dumont Dune Field, Mojave Desert, and numerical modeling, indicate that this complex pattern with high and variable slip values is associated with rover traverses in sands in which one or more wheels are trying to ascend the megaripple flanks. The increased drive actuator power needed to ascend megaripple flanks led to increased wheel actuator currents, increased slip, and in cases where one or more of the wheels carried more load, increased wheel sinkage and associated compaction resistance. Curiosity has since been directed to avoid these complex megaripple fields during its traverses.

The mobility difficulties experienced crossing complex megaripple fields were unexpected, and fortunately only a handful of sols were lost to automatic cessation of drives. The need to avoid these fields after the aborted Hidden Valley drives increased the time to reach Pahrump Hills, a site for which extensive scientific measurements were made (Vasavada et al., 2015), by ~30%, relative to what were thought to be relatively easy drives through valleys with megaripples. The Hidden Valley megaripple field is located in a transitional zone, whereas closer to Mount Sharp the extensive and active Bagnold Dune field will need to be detoured around and crossed where the dune sand is minimal. It remains to be seen how the rover will respond during these crossings. To prepare Artemis for more realistic high slip simulations of any future megaripple and dune crossings, the classical terramechanics model for wheel-sand interactions are being updated with more realistic discrete element method approaches (Johnson et al., 2015).

The problems associated with crossing megaripple fields have been acknowledged and are being studied by NASA's 2020 Mars Rover Team, in addition to consideration of updating Curiosity-style wheels for the 2020 rover with a thicker skin to minimize damage while driving over sharp rocks. Tests are also being conducted for both Curiosity and the 2020 rover using new ways of driving through megaripple and dune fields, including varying wheel currents based on sensed patterns associated with wheel burial and increased compaction resistance. Finally, the 2020 Mars Rover landing site selection team is including megaripple fields as likely hazards to avoid landing on and traversing across.

ACKNOWLEDGMENTS

We thank the Mars Exploration Program, Mars Science Laboratory (Curiosity rover mission), for support for the work presented in this paper. We also thank the many engineers and scientists associated with the Curiosity mission who have helped in one way or another to make the mission a success. We thank Fred Calef, JPL, for extensive work on HiRISE mosaic generation and co-registration with digital elevation maps generated from HiRISE stereo pair images.

REFERENCES

Arvidson, R. E., Gooding, J. L., & Moore, H. (1989). The Martian surface as imaged, sampled, and analyzed by the Viking Landers. Reviews of Geophysics, 27, 39–60.

Arvidson, R. E., Bell, J. F. III, Bellutta, P., Cabrol, N. A., Catalano, J. G., Crumpler, L., et al. (2010). Spirit Mars Rover Mission: Overview and selected results from the northern Home Plate Winter Haven to the side of Scamander Crater. Journal of Geophysical Research Planets, 115, E00F03, doi:10.1029/2010JE003633

Arvidson, R., Bellutta, P., Calef, F., Fraeman, A., Garvin, J., Gasnault, O., et al. (2014). Terrain physical properties derived from orbital data and the first 360 sols of Mars Science Laboratory Curiosity Rover Observations in Gale Crater. Journal of Geophysical Research Planets, 119, 1322–1344, doi:10.1002/2013JE004605

Bell, J. F. III, Malin, M. C., Caplinger, M. A., Ravine, M. A., Godber, A. S., Jungers, M. C., et al. (2012). Mastcam multispectral imaging on the Mars Science Laboratory Rover: Wavelength coverage and imaging strategies at the Gale Crater site. Lunar Planet. Sci. XLIII abstract 2541.

Bickler, D. B. (1988). Articulated suspension system, United States Patent US4840394 (A).

Christensen, P., Jakosky, B., Kieffer, H., Malin, M., McSween, H. Jr., Nealson, K., et al. (2004). The Thermal Emission Imaging System (THEMIS) for the Mars 2001 Odyssey Mission. In C. Russell (Ed.), 2001 Mars Odyssey (pp. 85–130), Netherlands, Dordrecht: Springer.

Blake, D., Morris, R., Kocurek, G., Morrison, S., Downs, R., Bish, D. et al. (2013). Curiosity at Gale Crater, Mars: Characterization and analysis of the Rocknest sand shadow. Science, 341, 1239505-1–1239505-7, doi:10.1126/science.1239505

Edgett, K., Yingst, R., Ravine, M., Caplinger, M., Maki, J., Ghaemi, F. et al. (2012). Curiosity's Mars Hand Lens

Imager (MAHLI) investigation. Space Science Reviews, 170(1-4), 259–317, doi:10.1007/s11214-012-9910-4

Fraeman, A., Arvidson, R. E., Ehlmann, B., Bridges, N., Clark, B., Cousin, A., et al. (2015). Physical and material properties of Gale Crater sandy deposits: From Rocknest to Pahrump. Lunar Planet. Sci. XLVI abstract 1682.

Grotzinger, J., Crisp, J., Vasavada, A., Anderson, R., Baker, C., Barry, R. et al. (2012). Mars Science Laboratory Mission and science investigation. Space Science Reviews, 170(1-4), 5–56, doi:10.1007/s11214-012-9892-2

Grotzinger, J., Summer, D., Kah, L., Stack, K., Gupta, S., Edgar, L., et al. (2014). A habitable fluvio-lacustrine environment at Yellowknife Bay, Gale Crater, Mars. Science, 343, 1242777-1–1242777-14, doi:10.1126/science.1242777

Haggert, S., & Waydo, J. (2008). The mobility system wheel design for NASA's Mars Science Laboratory Mission. 11th European International Society Terrain Vehicle Systems Meeting, Torino, Italy.

Heverly, M., Matthews, J., Lin, J., Fuller, D., Maimone, M., Biesiadecki, J. et al. (2013). Traverse performance characterization for the Mars Science Laboratory Rover. Journal of Field Robotics, 30(6), 835–846, doi:10.1002/rob.21481

Johnson, J., Kulchitsky, A., Duvoy, P., Iagnemma, K., Senatore, C., Arvidson, R., & Moore, J. (2015). Discrete element method simulations of Mars Exploration Rover wheel performance. Journal of Terramechanics, 31–41, doi: 10.1016/j.jterra.2015.02.004.

Maimone, M., Cheng, Y., & Matthies, L. (2007). Two years of visual odometry on the Mars Exploration Rovers. Journal of Field Robotics, 24(3), 169–186, doi:10.1002/rob.20184

Maki, J., Theissen, D., Pourangi, A., Kobzeff, P., Litwin, T., Scherr, L., et al. (2012). The Mars Science Laboratory engineering cameras. Space Science Reviews, 170, 77–93, doi:10.1007/s11214-012-9882-4

McEwen, A., Eliason, E., Bergstrom, J., Bridges, N., Hansen, C., Delamere, W., et al. (2007). Mars Reconnaissance Orbiter's High Resolution Imaging Science Experiment (HiRISE). Journal of Geophysical Research Planets, 112, E05S02, doi:10.1029/2005JE002605

Moore, H. J. (1987). Physical properties of the surface materials at the Viking Landing sites on Mars. United States Geological Survey Professional Paper 1389, 222 p.

Nakashima, H., & Kobayashi, T. (2014). Effects of gravity on rigid rover wheel sinkage and motion resistance assessed using two-dimensional discrete element method. Journal of Terramechanics, 53, 37–45, doi: 10.1016/j.jterra.2014.03.004

Senatore, C., Stein, N., Zhou, F., Bennett, K., Arvidson, R., Trease, B., et al. (2014). Modeling and validation of mobility characteristics of the Mars Science Laboratory Curiosity Rover. Paper presented at 2014 i-SAIRAS, Montreal, June 2014.

Stein, N., Arvidson, R., Heverly, M., Lindemann, R., Trease, B., Iagnemma, K., & Senatore, C. (2013). Validation of Artemis mobility simulations for the Spirit, Opportunity, and Curiosity Mars rovers. American Geophysical Union Fall Meeting, Abstract P51G-1826.

Sullivan, R., Anderson, R., Biesiadecki, J., Bond, T., & Stewart, H. (2011). Cohesions, friction angles, and other physical properties of Martian regolith from Mars Exploration Rover wheel trenches and wheel scuffs. Journal of Geophysical Research Planets, 116, E02006, doi:10.1029/2010JE003625

Sullivan, R., & Zimbelman, J. (2015). Megaripples and their sedimentary deposits on Earth and Mars. Lunar Planet Sci. XLVI abstract 2762.

Tehari, S. H., Sandu, C., Taheri, S., Pinto, E., & Gorsich, D. (2015). A technical survey on terramechanics models for tire–terrain interaction used in modeling and simulation of wheeled vehicles. Journal of Terramechanics, 57, 1–22, doi:10.1016/j.jterra.2014.08.003

Vasavada, A., & Science Team, M. S. L. (2015). Latest results from the Mars Science Laboratory Mission and Curiosity Rover. Lunar Planet Sci. XLVI abstract 2715.

White, C., Antoun, G., Brugarolas, P., Lih, S., Peng, C., Phan, L., San Martin, A., et al. (2012). System verification of MSL Skycrane using an integrated ADAMS simulation. Paper presented at proceedings of 2012 IEEE Aerospace Conference, March 2012, doi:10.1109/AERO.2012.6186994

Williams, R., Grotzinger, J., Dietrich, W., Gupta, S., Sumner, D., Wiens, R., Mangold, N., et al. (2013). Martian fluvial conglomerates at Gale Crater. Science, 340, 1068–1072, doi:10.1126/science.1237317

Wong, J. (2001). Theory of ground vehicles (3rd ed.). New York: John Wiley & Sons.

Wong, J. (2012). Predicting the performances of rigid rover wheels on extraterrestrial surfaces based on test results obtained on earth. Journal of Terramechanics, 49, 49–61, doi:10.1016/j.jterra.2011.11.002

Zhou, F., Arvidson, R., Bennett, K., Trease, B., Lindemann, R., Bellutta, P., et al. (2014). Simulations of Mars rover traverses. Journal of Field Robotics, 31(1), 141–160, doi:10.1002/rob.21483